PNAS RESEARCH ARTICLE | MICROBIOLOGY

SypC, a symbiont outer membrane vesicle protein, impacts the development of the squid–vibrio partnership

Jill T. Kuwabara[a,b], Vera Beilinson[c], Alexis C. Hargadon[b], Grischa Y. Chen[b,c], Xiao-Meng Hu[b,c], Mark S. Ladinsky[c], Kathleen T. Hackett[d], Joseph P. Dillard[d], Karen L. Visick[e], Edward G. Ruby[a,c], and Margaret McFall-Ngai[a,b,c,1]

Affiliations are included on p. 9.

Contributed by Margaret McFall-Ngai; received September 3, 2025; accepted February 9, 2026; reviewed by Anne M. Krachler and George O'Toole

Bacterial outer membrane vesicles (OMVs) and the cargo they carry are increasingly recognized as a means of communication between microbial symbionts and the cells of their host. However, few studies have focused on the biochemical and molecular mechanisms underlying OMV signaling during symbiosis onset and development. We show here that SypC, an OMV protein of the bioluminescent symbiont *Vibrio fischeri,* is taken up by cells of the squid host *Euprymna scolopes* where it assumes a new function, i.e., the facilitation of symbiont-induced light-organ morphogenesis. SypC is a Wza-like outer membrane protein found in host-associated Vibrionaceae and is essential for *V. fischeri* biofilm formation. Colonization or direct treatment with *V. fischeri* OMVs triggers host development, which was reduced or delayed if the host is instead exposed to a Δ*sypC* mutant or Δ*sypC* OMVs. RNA-seq analyses comparing light organs colonized by either the mutant or its parent revealed differential expression of host genes associated with immune responses and tissue morphogenesis. In immunocytochemical imaging, SypC-bearing OMVs were taken up by the host's macrophage-like cells near the light-organ crypts, revealing the mechanism by which SypC travels through tissue to trigger morphogenesis. Taken together, the data provide evidence that in addition to its role in biofilm formation and colonization, SypC has a second function promoting the induction of symbiotic-tissue development. These findings provide a critical piece of a puzzle whereby a rich array of host and symbiont molecules work in concert to orchestrate normal symbiont colonization and host development within the first hours to days of symbiosis.

OMVs | transcriptomics | symbiosis | *Euprymna scolopes* | *Vibrio fischeri*

Significance

Bacterial symbionts can profoundly influence host development. Using the *Euprymna scolopes-Vibrio fischeri* model symbiosis, this study provides evidence for recruitment of the outer membrane protein SypC, which is necessary for *V. fischeri* biofilm formation, into the process of host morphogenesis that occurs early in the symbiosis. This divergent dual-function role that SypC plays requires it to be shed from the cell surface of *V. fischeri* in outer membrane vesicles (OMVs). Host macrophage-like cells phagocytose and traffic the OMVs to a distant site where they are essential for induction of light-organ development. Because many species of the Vibrionaceae share unusual structural features of SypC, this protein may be critical for host–vibrio interactions in both nonpathogenic and pathogenic associations.

Most, if not all, Gram-negative bacteria produce outer membrane vesicles (OMVs), which have recently been recognized to be involved in communication with host cells (for review, see refs. 1–3). For many species, OMVs are released from the bacterial cell surface by a nonlytic budding mechanism of the outer membrane (2, 4) that can be recognized by the almost solely periplasmic and outer membrane derivation of their proteome (e.g., refs. 5, 6). The cargo present in OMVs also includes nucleic acids and components of the outer envelope, such as lipopolysaccharide (LPS) and peptidoglycan (PGN) derivatives. Following release from the cell surface of bacterial symbionts, these vesicles interact with surface receptors on host epithelial or blood cells, or can even enter the cytoplasm, where they are often recognized by intracellular receptors. Increasing evidence suggests that OMVs internalized in host cells can release their cargo into the host-cell cytoplasm and influence the function and viability of those cells (6–8). OMVs have been principally characterized in bacterial pathogenesis (9, 10), but recent studies have shown them to be critical elements of beneficial symbioses of both vertebrates (6) and invertebrates (see, e.g., refs. 11–13). For example, OMVs of the microbiota have been shown to enter the bloodstream of mammals, where they influence host immunity and disease response (12, 14), as well as to cross the blood–brain barrier, where they influence neurological health and disease (15).

Studies of the squid–vibrio model symbiosis have provided insights into the involvement of symbiont OMVs in modulating host–microbe interactions (16, 17). Host exposure to either ^{15}N-labeled *V. fischeri* cells or OMVs derived from these cells results in indistinguishable patterns of heavy-isotope labeling of the host tissues (7). In this system, the luminous bacterium *Vibrio fischeri* resides in crypt spaces along the apical epithelium of the symbiotic light-emitting organ of the Hawaiian bobtail squid, *Euprymna scolopes* (18, 19). Each generation, the aposymbiotic (APO) (i.e., symbiont-free) light organ of the newly hatched juvenile host specifically recruits *V. fischeri* cells from the bacterioplankton within hours; these founders and their progeny remain the symbionts throughout the squid's lifespan. The host hatches with a light-organ morphology that potentiates symbiont

Author contributions: J.T.K., V.B., G.Y.C., J.P.D., K.L.V., E.G.R., and M.M.-N. designed research; J.T.K., V.B., A.C.H., G.Y.C., X.-M.H., M.S.L., K.T.H., and K.L.V. performed research; J.P.D. and K.L.V. contributed new reagents/analytic tools; J.T.K., V.B., A.C.H., G.Y.C., X.-M.H., M.S.L., K.T.H., J.P.D., K.L.V., E.G.R., and M.M.-N. analyzed data; and J.T.K., V.B., A.C.H., G.Y.C., M.S.L., J.P.D., K.L.V., E.G.R., and M.M.-N. wrote the paper.

Reviewers: A.M.K., The University of Texas Health Science Center at Houston; and G.O., Dartmouth College Geisel School of Medicine.

The authors declare no competing interest.

[1]To whom correspondence may be addressed. Email: mcfallng@caltech.edu.

This article contains supporting information online at https://www.pnas.org/lookup/suppl/doi:10.1073/pnas.2524648123/-/DCSupplemental.

Published March 11, 2026.

recruitment (Fig. 1*A*). Ciliated fields on the nascent symbiotic organ entrain environmental *V. fischeri* cells above pores on the organ surface (Fig. 1 *A'*, *Left*). These cells aggregate in host-derived mucus (Fig. 1*A"*). This behavior requires the production of an exopolysaccharide on the surface of *V. fischeri* cells, a function that is encoded by the symbiont's *syp* locus (20). Thus, the biofilm consists of two components: host mucus and the bacterial exopolysaccharide. After aggregating, the cells migrate through host tissues to colonize the crypt spaces (Fig. 1 *A'*, *Right*), where they induce the loss of the superficial ciliated fields over the first 4 to 5 d following colonization (18). This gradual process involves two conspicuous phenotypes: i) widespread cell death of the superficial ciliated cells (Fig. 1*B*); and ii) the migration of squid-host macrophage-like blood cells, or hemocytes, into the blood sinuses of the ciliated-appendage epithelia (Fig. 1*C*). Following an upregulation of matrix metalloprotease activity in the basement membrane (21), the dying cells are sloughed from the surface, i.e., they are not phagocytosed by the hemocytes in the blood sinus. The microbe-associated molecular patterns, or MAMPs, present in the OMVs of *V. fischeri* cells, specifically LPS and PGN derivatives, trigger most of this cell death and hemocyte migration, with symbiont light production being required for the full developmental program (22). While LPS and PGN are common to many bacterial species, this response is specific to *V. fischeri* because the signals originate in light-organ crypts, where only this species can persist (16, 23). Whereas a great deal of this process has been described, the mechanism by which the inductive message is transferred from the bacteria in the crypt spaces to the superficial ciliated fields has remained unresolved.

Investigations of *V. fischeri* OMVs have shown that LPS, as well as hundreds of proteins and several RNA types (tRNA, rRNA, and small noncoding RNAs or sRNAs), are trafficked into host cells. Thus far, three of these biomolecules in the OMVs have been deeply characterized, i.e., the LPS (24), the sRNA SsrA, also called tmRNA (17), and the outer membrane protein OmpU (5). The data showed that these molecules each impact a specific feature of early symbiosis development.

In this study, we present data from an examination of the importance of SypC [See *SI Appendix*, Fig. S1*A*; UniProt (25)], a *V. fischeri* protein present in the OMVs (26) (*SI Appendix*, Fig. S1*B*), on host light-organ gene expression and development. SypC was selected for study because there is a deep understanding of components of the *V. fischeri syp* locus (20), which encodes proteins that produce an exopolysaccharide critical in symbiosis competency. SypC is an intrinsic outer membrane–spanning protein that is a paralog of the *V. fischeri* GfcE and its ortholog *Escherichia coli* Wza (*SI Appendix*, Fig. S1*A*) (27). It is essential for the export of the bacterium's exopolysaccharide (EPS) or Syp polysaccharide (28) and is the only protein encoded by the *syp* locus that is detected in OMVs (5). The data presented here provide evidence that SypC is critical for conveying the information that potentiates host light-organ development and promotes colonization of the crypts by *V. fischeri*.

Results

Δ*sypC*-Colonized Light Organs Have Altered Transcriptional Responses. To understand how colonization by a Δ*sypC* symbiont might differentially influence host gene expression, we performed an RNA-seq experiment at 24 h postinoculation (hpi). Relative to APO animals, *V. fischeri* colonization, regardless of the presence of *sypC* in the symbionts (i.e., WT or Δ*sypC*), modulated the expression of 396 genes, clearly distinguishing uncolonized squid from symbiotic ones. (Fig. 2 *A*, *Left*, and *B*). This result is not unexpected, as multiple factors from *V. fischeri* (e.g., MAMPs and light production) are known to modulate host gene expression (22). Nevertheless, the presence of *sypC* did have a clear transcriptional impact, specifically affecting a distinct subset of host genes. Differential expression (DE) analysis (see PERMANOVA, in *SI Appendix*, *Supplemental Results*) comparing colonization by either the WT or the Δ*sypC* strain identified 138 *sypC*-dependent regulated genes (green and yellow, Fig. 2*B*). Hierarchical clustering showed that these genes had similar expression levels in APO and Δ*sypC* treatments, indicating that to be regulated, these genes require the presence of *sypC* in the symbionts (Fig. 2 *C*, *Left*). Additionally, we identified 345 genes that were not significantly different after WT or Δ*sypC* colonization but instead exhibited an intermediate level of expression in Δ*sypC* relative to WT and APO (Fig. 2 *C*, *Right*). These genes were statistically DE between

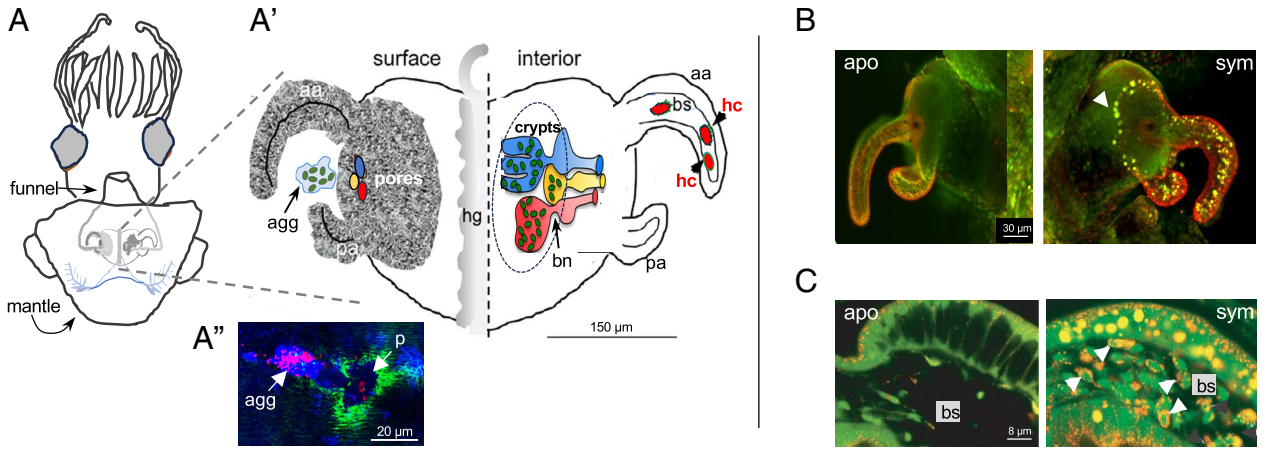

Fig. 1. Juvenile light organ features and colonization developmental events. (*A*) The morphology and anatomy of the symbiotic organ. Ventral view of an *E. scolopes* showing the location of the light organ beneath the mantle and funnel. (*A'*) Expanded diagram of the light organ. *Left half:* surface features of the organ, showing the superficial ciliated fields (gray) and three pores, relative to the position of the hindgut (hg). *V. fischeri* cells (green) in the ambient seawater aggregate in mucus outside of the pores (agg). *Right half:* internal regions of the organ including 3 crypts and the migration-pathway bottlenecks at their entrances (one indicated, bn). *V. fischeri* cells (green) are located in the crypts; the blood sinuses (bs) of the superficial ciliated appendages (aa, anterior appendage; pa, posterior appendage) contain migrating hemocytes (hc, red). (*A"*) Confocal image of aggregated *V. fischeri* cells (magenta) in host mucus (blue) outside of a pore (p) surrounded by cilia (green). (*B*) Once the light organ is colonized, the superficial ciliated fields regress by programmed cell death; dying cells (yellow puncta) were visualized by acridine orange staining, characteristic of early stage cell death of symbiotic (sym) but not aposymbiotic (apo) light organs. (*C*) Close-up images of tissues of the blood sinuses (bs) of the ciliated appendages. After colonization by *V. fischeri* cells, the blood sinuses fill with hemocytes (white arrowheads).

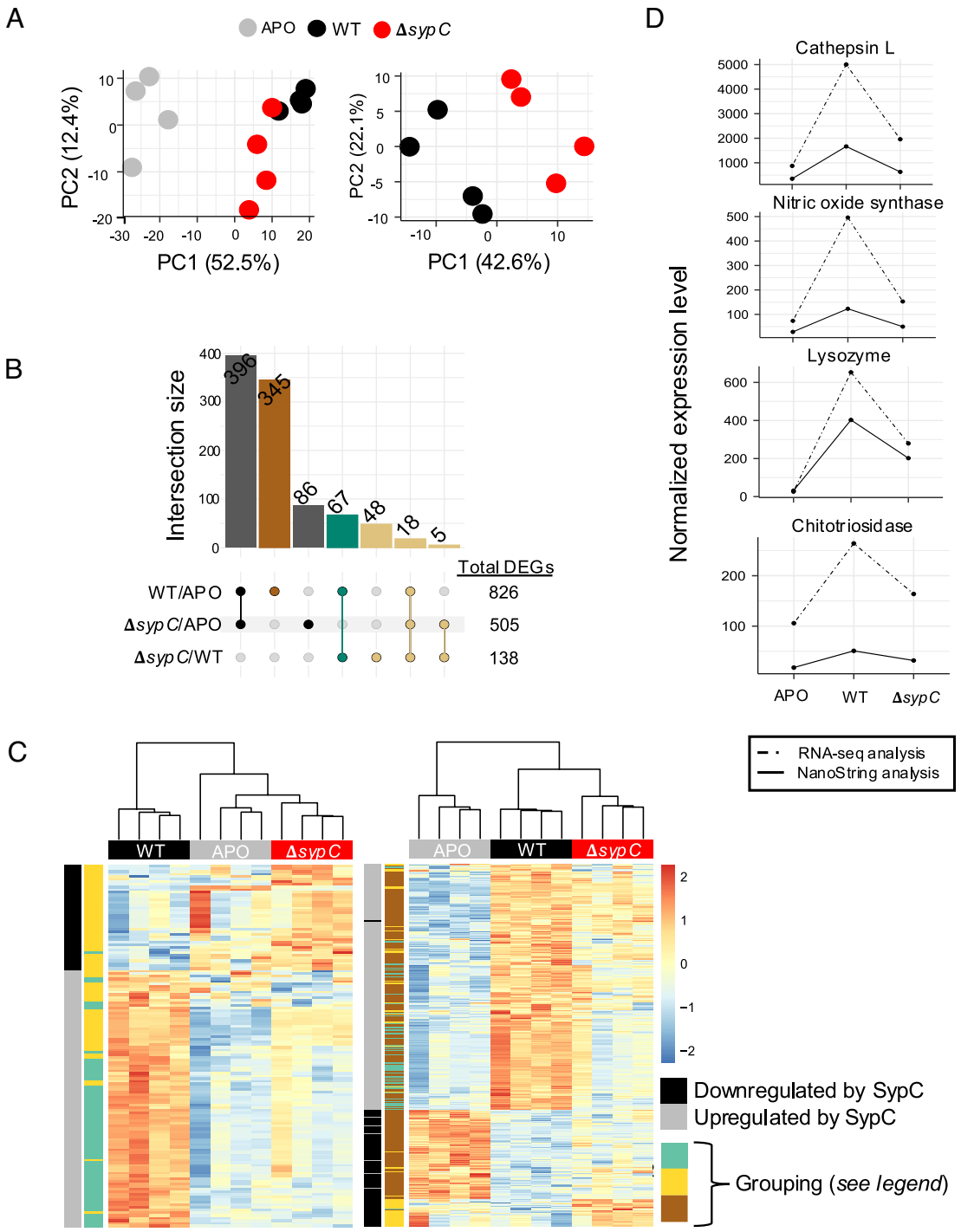

Fig. 2. Relative impact of the Δ*sypC* mutant on light-organ gene expression. (*A*) Principal component analysis (PCA) of host transcriptomes. *Left*: three conditions are shown: uncolonized (APO, gray), colonized with wild-type bacteria (WT, black), or colonized with the Δ*sypC* mutant (Δ*sypC*, red). *Right*: Same data as *Left*, but with APO excluded to better highlight the separation between WT and Δ*sypC*. Percent variance explained by each principal component is indicated on the axes. (*B*) UpSet plot of differentially expressed genes (DEGs). Comparisons include WT vs. APO and Δ*sypC* vs. APO ($\log_2$ FC ≥ |1|, adjusted $P < 0.05$), and Δ*sypC* vs. WT ($\log_2$ FC ≥ |0.58|, adjusted $P < 0.05$). (*C*) Expression patterns of selected DEG categories. *Left*: Green and yellow genes highlight that Δ*sypC* colonized animals resemble APO more closely for this subset. *Right*: Green, yellow, and brown gene groupings illustrate that Δ*sypC* represents an intermediate expression state between APO and WT. *Color coding:* Black: Downregulated by SypC (Δ*sypC* > WT). Gray: Upregulated by SypC (Δ*sypC* < WT). Green: DE in both WT vs. APO and Δ*sypC* vs. WT. Yellow: DE only in Δ*sypC* vs. WT. Brown: DE only in WT vs. APO. (*D*) Expression validation of selected genes comparing RNA-seq and NanoString analyses.

WT/APO, but not between either Δ*sypC*/APO or Δ*sypC*/WT (brown, Fig. 2*B*). Such a pattern suggests that *sypC* contributed to achieving full expression of these genes.

Examining all genes of interest (Fig. 2; brown, yellow, and green), GO-term enrichment analysis highlights the possibility that symbiont carriage of *sypC* suppresses pathways related to cytoskeletal organization and cellular motility, and upregulates host responses involved in metabolism, immune modulation, cell adhesion, and extracellular remodeling (*SI Appendix*, Fig. S2), including production of a matrix metalloprotease by the ciliated epithelium, which is increased 24 h after colonization and is involved in light-organ morphogenesis (29). Twenty-five other upregulated host genes of interest were associated with cell death and proteolysis (*SI Appendix*, Fig. S3 *A* and *B*), supporting the

idea that the presence of the SypC protein promotes host-cell death in the ciliated fields (Fig. 3*A*).

To validate the RNA-seq results, NanoString analysis was performed on selected targets (Fig. 2*D* and *SI Appendix*, Fig. S3*C*). Previously studied symbiosis-associated genes such as cathepsin L, nitric oxide synthase, lysozyme, and chitotriosidase (reviewed in ref. 18) were upregulated by symbionts encoding SypC, consistent with both cell-death enhancement and immune-response modulation. Most of these crucial developmental genes were downregulated in a colonization by a Δ*sypC* mutant compared to WT, further highlighting the importance of SypC during tissue morphogenesis.

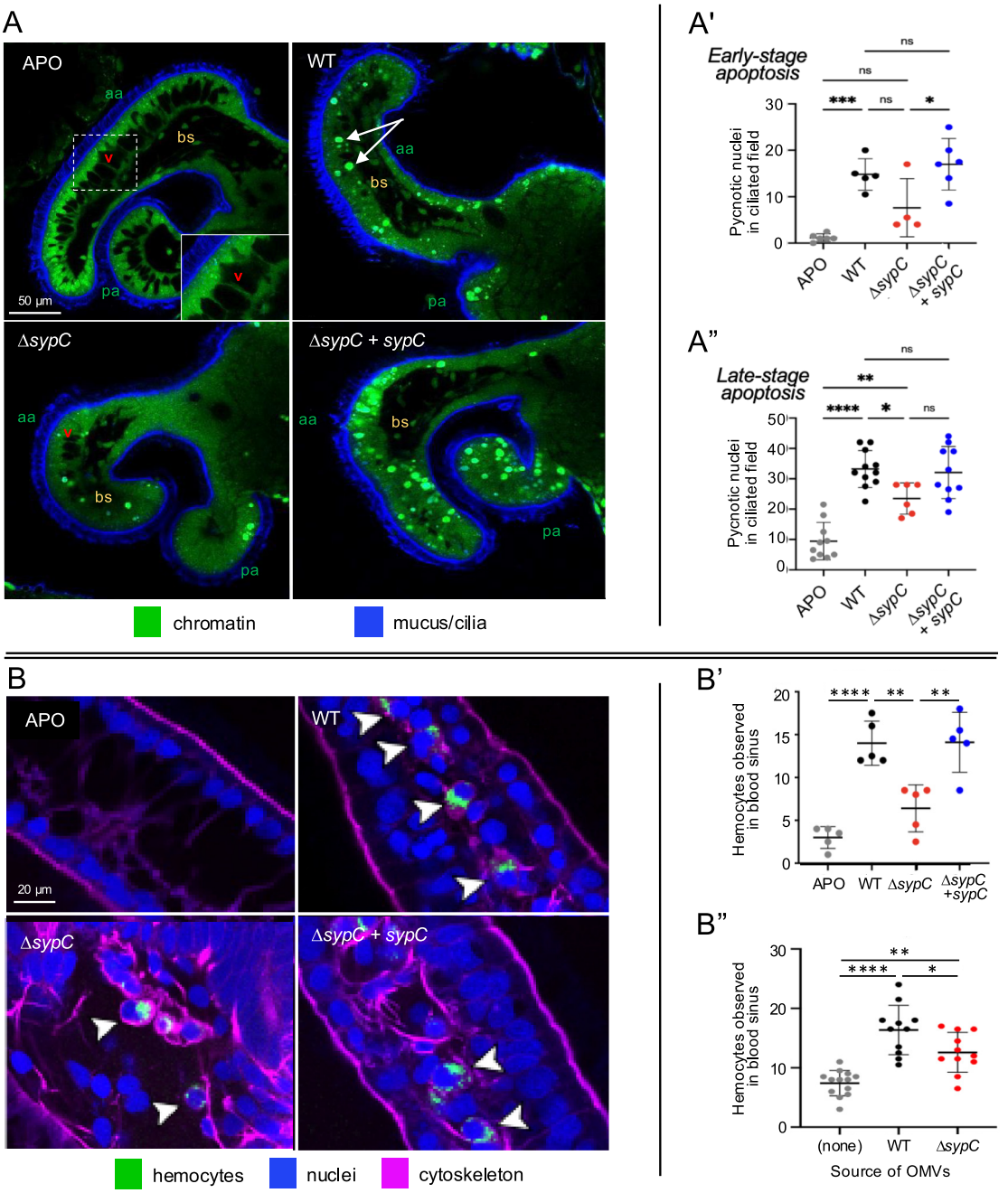

Fig. 3. Colonization by the *V. fischeri* Δ*sypC* mutant attenuates normal cellular phenotypes of the host. (*A*) Representative images of the superficial ciliated fields of light organs that were APO or colonized with wild-type *V. fischeri* (WT), Δ*sypC*, or the complemented Δ*sypC* +*sypC* strains. At 24 h postcolonization, levels of symbiosis-induced early-stage apoptosis were determined in the ciliated field with each condition, as indicated by pycnotic nuclei (condensed chromatin, e.g., white arrows) in these regions. Fluorochromes used: cell death was indicated by acridine-orange stained condensed chromatin (green); mucus was stained with wheat-germ agglutinin (blue). aa, anterior appendage; bs, blood sinus; pa, posterior appendage; v, vacuoles within the lateral epithelial cells of the ciliated field. (*A'*) Quantification of nuclei indicating early-stage cell death. (*A"*) Quantification of late-stage apoptosis was determined using the fluorochrome TUNEL (terminal deoxynucleotidyl transferase dUTP nicked-end labeling). (*B*) Representative images of hemocytes (blood cells, white arrowheads) trafficking into the blood sinus of the anterior appendage under the four colonization conditions. Fluorochromes used: hemocytes were identified by DNase-1 staining (green); F-actin cytoskeleton was stained with phalloidin (magenta); nuclei, TO-PRO-3 (blue). (*B'*) The number of hemocytes present in the blood sinus of the anterior appendage was quantified at 24 h after colonization by different *V. fischeri* strains. (*B"*) Hemocyte trafficking was also determined in animals exposed only to OMVs that had been isolated from either WT or Δ*sypC* strains. For all conditions in *A'* and *A"*, and *B'* and *B"* each data point represents a biological replicate. Each experiment was repeated 3 times with the same outcome. Results are presented as mean ± 1 SD. Comparisons between multiple groups were analyzed using one-way ANOVA with Tukey test. ns: not significant, $P > 0.05$; *$P \le 0.05$; **$P \le 0.01$; ***$P \le 0.001$; ****$P \le 0.0001$.

Colonization by the Δ*sypC* Mutant Affects Certain Features of Host Development. In response to colonization by the Δ*sypC* mutant, several typical wild-type-induced developmental phenotypes were significantly reduced (Fig. 3). Both early-stage (characterized by condensed chromatin; Fig. 3 *A* and *A'*) and late-stage (characterized by fragmented chromatin; Fig. 3*A"*) cell death were often statistically different; however, due to natural genetic variation of juveniles during development, some clutches only showed significant differences during late-stage cell death. Similarly, the number of hemocytes migrating into the blood sinuses of the anterior appendages of the ciliated fields was consistently statistically reduced in Δ*sypC*-colonized animals (Fig. 3 *B* and *B'*). Treatment of juveniles with *V. fischeri* OMVs was sufficient to induce the migration of hemocytes to the blood sinus (23), even in the absence of the bacteria themselves (Fig. 3*B"*), indicating that OMVs alone were adequate to trigger this key developmental event. Further, the reduced level of hemocyte migration that resulted from a Δ*sypC* colonization (Fig. 3*B'*) was phenocopied when animals were exposed to OMVs produced by the mutant strain relative to wild-type OMVs (Fig. 3*B"*).

SypK, another protein encoded by the *syp* locus and essential for biofilm formation (28), contains the conserved RfbX flippase domain found in Wzx (30). It likely transports subunits of the Syp polysaccharide from the cytoplasm into the periplasm where they are assembled. SypK is predicted to be associated with the cytoplasmic membrane and thus, unlike the outer membrane SypC, was not detected in OMVs (5). In contrast to the Δ*sypC* mutant, colonization by the Δ*sypK* mutant did not significantly affect the level of hemocyte migration (*SI Appendix*, Fig. S4). These results indicate that it is the absence of the SypC protein itself, not a disruption of exopolysaccharide production, that is responsible for the inability of Δ*sypC* to induce normal hemocyte migration.

Certain other morphological events in the developmental program are also absent or delayed in Δ*sypC* colonized animals, such as the loss of the ciliated ridge on the light organ's surface (31) (*SI Appendix*, Fig. S5*A*) at 24 hpi. However, squids colonized by Δ*sypC* did retain several other normal developmental phenotypes, such as the typical regression of the superficial ciliated fields, which did not differ significantly between WT- and Δ*sypC*-colonized animals at 72 hpi (*SI Appendix*, Fig. S5 *B–D*). In addition, a phenotype occurring more deeply in the symbiont's migration path, i.e., the symbiont-induced closure of the migration path "bottleneck" (32, 33), was similar in animals colonized by either the WT or Δ*sypC* strain (*SI Appendix*, Fig. S5*E*).

Given that the peptidoglycan monomer TCT (tracheal cytotoxin) induces hemocyte migration into the blood sinuses of the appendages (26), we hypothesized that the Δ*sypC* would be deficient in TCT production. To test this notion, we measured the amount of TCT produced by WT and Δ*sypC* cells in culture and determined that the mutant produced roughly the same level of TCT as the WT strain (See *SI Appendix*, Fig. S6 *A* and *B*). This result suggests that the developmental defect caused by the Δ*sypC* symbiont is not in the production of TCT but instead in the ability of this TCT to induce hemocyte migration normally. Interestingly, the experimental addition of high levels of TCT directly to seawater can itself induce hemocyte migration in both uncolonized and Δ*sypC*-colonized animals (*SI Appendix*, Fig. S6*C*), indicating that such a pharmacological treatment with TCT alone can be sufficient to overcome the typical requirement that SypC be present to enable induction of hemocyte migration.

Symbiont SypC Protein Is Found within Host Hemocytes. Because the SypC protein itself is required for normal host responses to either colonization by symbionts or treatment with OMVs, we investigated whether this protein's effect was due to accumulation within host cells. Prior studies have shown that components of symbiont-produced OMVs can enter host cells, including LPS, which induces early-stage cell death (24), and small RNAs (17). These findings suggest a mechanism by which OMV-associated SypC (5) could also be delivered into host cells. To determine whether SypC is, in fact, translocated within the light organ, we introduced into wild-type *V. fischeri* a gene encoding an mCherry-SypC fusion protein that was constitutively expressed from its plasmid (*SI Appendix*, Table S1). Thus, this SypC fusion protein was well expressed, functional, and could easily be detected in bacterial cell extracts using a fluorescent antibody made against mCherry (*SI Appendix*, Fig. S7). When juvenile animals were examined at 24 hpi, the SypC fusion protein was observed within the colonized light organ by immunocytochemistry using an anti-mCherry antibody (Fig. 4). As expected, the symbionts themselves were strongly labeled. The SypC fusion protein was also observed in the cytoplasm of the epithelial cells lining the crypts (Fig. 4*A*); however, when colonized by wild-type symbionts carrying mCherry alone, no antibody reaction was observed in hemocytes (*SI Appendix*, Fig. S8), indicating that these cells internalize OMVs, but not entire *V. fischeri* symbionts. Further, the SypC-fusion labeling was in proximity to the nucleus, but excluded from the nuclear region (Fig. 4 *B* and *C*). Examination of tissues distant from the crypts revealed labeled SypC (Fig. 4 *D–G"*) appearing even as remotely as the blood sinus of the external ciliated appendages (Fig. 5*A*). In colonized animals, hemocytes migrate to the appendages prior to the onset of cell death (34); thus, we asked whether SypC might be associated with these tissue-targeting cells and, if so, whether the presence of SypC might be connected to cell-death-driven morphogenesis.

Colocalization of the SypC label with a hemocyte-specific marker confirmed that this symbiont protein was internalized and carried into the sinuses of the appendages by these host cells (Fig. 4 *D* and *E–E"*). We next hypothesized that the SypC protein entered the phagocytic hemocytes through the uptake of symbiont OMVs they encountered while traversing the crypts (18). We tested this by asking whether OmpU, another symbiont protein present in OMVs (5), also colocalized with the hemocytes in the appendages. As predicted, an antibody to an mCherry-OmpU fusion protein labeled these host cells (Fig. 4 *F* and *G–G"*), indicating that the uptake of SypC was not specific to that protein, and likely occurred during the phagocytosis of OMVs.

The Progression of SypC Transported to the Blood Sinuses by Migrating Hemocytes Is Associated with the Induction of a Proteolytic Gene. The path of SypC-containing hemocytes was tracked from the light-organ crypts to the blood sinuses of the superficial ciliated appendages. At 9 hpi, SypC was first observed in the hemocytes near the crypt spaces, presumably after they had phagocytosed symbiont OMVs (Fig. 5 *A–D*). By 12 hpi, labeled hemocytes were most easily detected distally near the region of the pores (Fig. 5*E*). Finally, by 17 hpi, hemocytes containing SypC were primarily in the blood sinuses of the appendages (Fig. 5*F*). Hemocytes collected from symbiotic animals at 24 hpi had increased levels of the C8 subunit of the proteasome, a proteolytic complex that is induced in hemocytes of the wild-type colonized light organ during cell death of the appendages (35). In contrast, no such induction was seen in hemocytes collected from Δ*sypC* colonized squid (Fig. 5*G*).

Discussion

SypC is a putative outer membrane transport protein involved in Syp-polysaccharide secretion and biofilm formation, activities that are critical for the initiation of symbiosis by planktonic *V. fischeri*

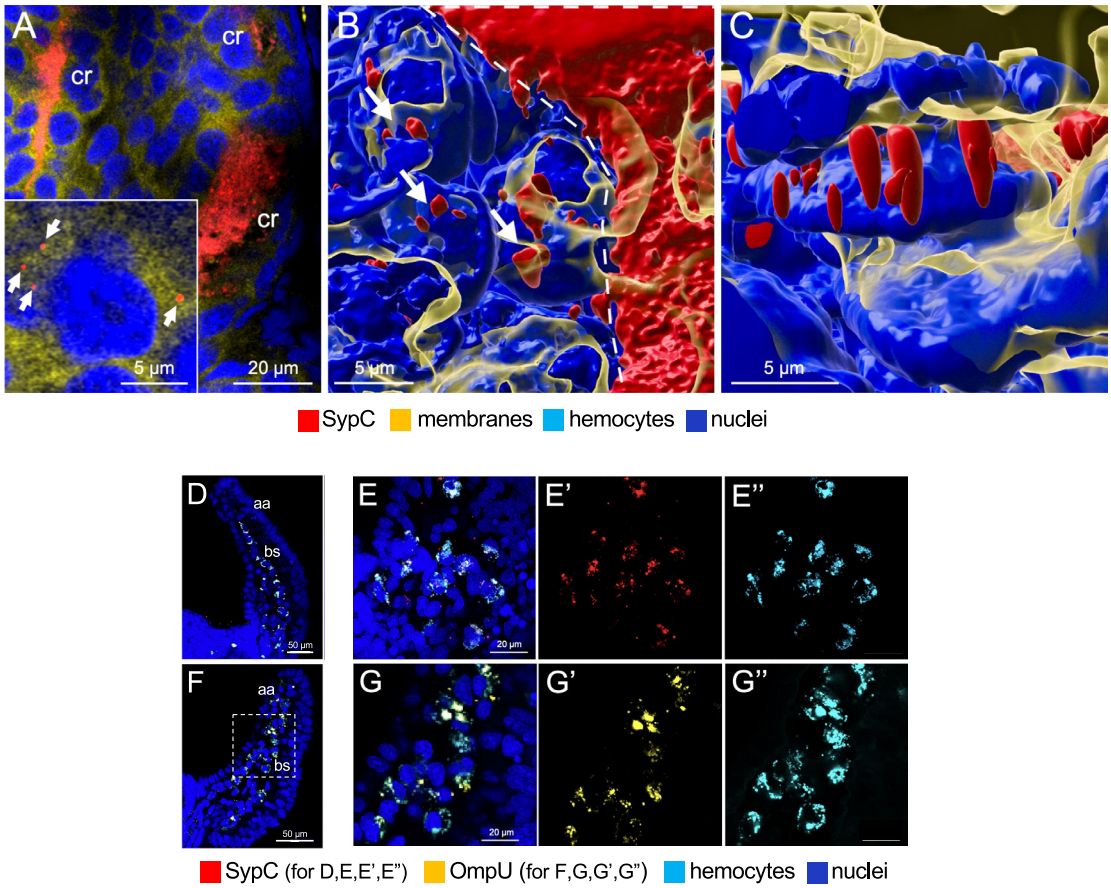

Fig. 4. Components and activities of migrating hemocytes. Localization of SypC within and near the symbionts at 24 hpi. (*A*) Abundance of antibody labeling of *V. fischeri* SypC in the light-organ crypt spaces (cr). *Insert,* mCherry-SypC fusion protein detected by fluorescent mCherry antibody (white arrows) within the cytoplasm of host cells lining the crypts. (*B*) Imaris rendering of higher-magnification confocal images showing SypC (white arrows) within host cells in regions near nuclei. The dashed line indicates the boundary between the host cells (*Left*) and the symbiont-containing crypts. CellMask Orange-stained membranes in and surrounding the cytoplasm. (*C*) Imaris rendering demonstrating that SypC is extranuclear. (*D*) Labeling of the *V. fischeri* SypC-fusion protein within the blood sinus (bs) of an anterior appendage (aa) of the superficial ciliated field of the organ; low magnification image showing the general location of higher magnification area. (*E–E"*) Higher magnification images showing the association of SypC with hemocytes in the blood sinus. DAPI-stained nuclei, (blue); fluorescent antibody to mCherry portion of mCherry-SypC fusion protein (red); CellMask Orange-stained hemocytes (turquoise). (*F*) Labeling of the *V. fischeri* OmpU protein within the blood sinus; low magnification image as in *D*. (*G–G"*) Higher magnification images showing the association of OmpU with hemocytes in the blood sinus. DAPI-stained nuclei, (blue); fluorescent antibody to OmpU (yellow); CellMask Orange-stained hemocytes (turquoise). Images of experimental controls can be found in *SI Appendix*, Fig. S8.

cells (for review, see ref. 20), as well as for their colonization of the light organ (36). Recent studies have shown that, of the 18 proteins encoded by the well-studied *syp* locus, SypC is the only one that is present in *V. fischeri* OMVs (5), likely due to its being embedded within the outer membrane. Here, we present data on host phenotypes that rely on the presence of SypC for normal symbiosis onset. Expression of hundreds of juvenile-host genes is dependent on colonization by symbionts that encode SypC (Fig. 2). Further, in the early hours of the host–symbiont partnership, SypC-bearing OMVs are taken up by phagocytic blood cells, or hemocytes, of the juvenile host and trafficked through its tissues to the outer surface of the light organ. The SypC delivered to the surface is essential for inducing, either directly or indirectly, normal development of the symbiosis.

Prior to the work described here, the presence of symbiont OMVs in the bloodstream of the squid host (17) had suggested that bacterial proteins like SypC, present in phagocytosed OMVs, might impact not only the light organ, but other tissues as well (37). Our findings add to the growing recognition that OMV trafficking through the body of a host is an evolutionarily conserved mechanism of host–symbiont communication (38, 39). Such long-range trafficking of OMVs has been documented in a variety of eukaryotic hosts spanning from plants, choanoflagellates, and sponges to squids and vertebrates (5, 6, 40, 41). In mammals, not only do OMVs of the gut microbiome have either beneficial or pathologic influences locally on the gastrointestinal epithelium, they also cross into the bloodstream where they are transported to distant tissues with wide-ranging effects (for reviews, see refs. (42, 43)). Recent studies of pregnant women have provided evidence that this phenomenon even occurs with the delivery of OMVs from the mother's microbiota to the developing fetus (44). Once the OMVs are delivered, they can have an array of effects (38). For example, notable here is the role of the *V. fischeri* OMVs in inducing normal cell death in the light organ's superficial ciliated epithelium (45); such OMV-induced cell death has also been reported in a diversity of other host animals, from sponges to mammals (40, 46).

The activity of SypC in bacterial-induced animal development is only one of a variety of bacterial and host features that work in concert to promote a normal and productive symbiosis. SypC is unusual in that its role in inducing host development is so distinct from its role in biofilm secretion. Proteins that have taken on a divergent role have been termed as "dual-function" (see, e.g., ref. 47). These proteins are not uncommon within a bacterial species, or between bacterial species,

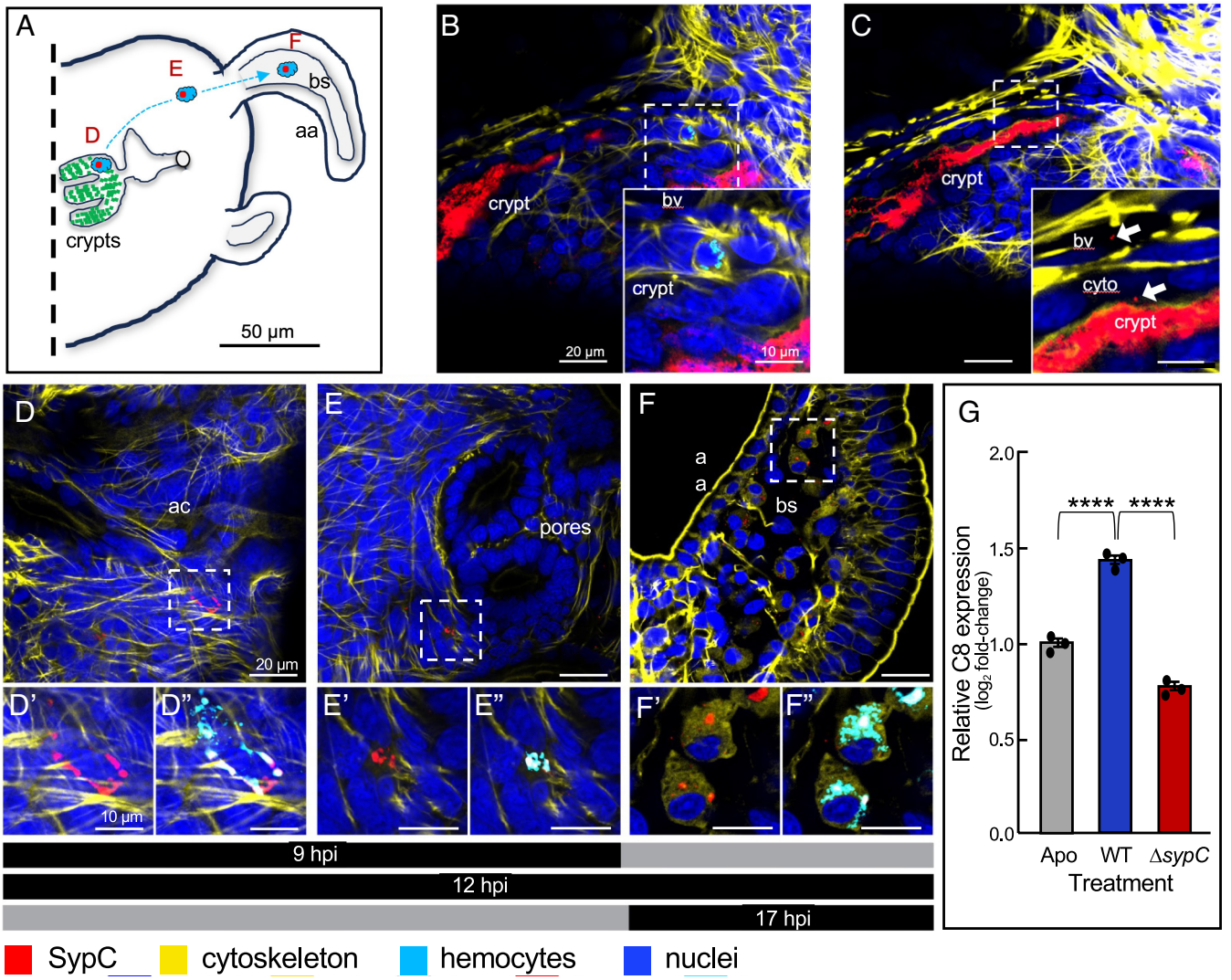

Fig. 5. Migration of SypC-bearing hemocytes to the blood sinus. (*A*) Tracking of host hemocytes during the first 17 h postinfection (hpi) as they migrate from the crypts to the blood sinus (bs) of the anterior appendage (aa). The presence of SypC-bearing hemocytes was indicated by the colocalization of a mCherry-SypC fusion protein (red) detected by a fluorescent mCherry antibody, with the CellMask Orange-stained hemocytes (turquoise). The hemocytes were observed near the medial crypt tissues at 9 hpi (*B–D*), progressed through the lateral tissues of the light organ by 12 hpi (*E*), and became situated in the blood sinus of the anterior appendage as soon as 17 hpi (*F*). The areas indicated by the dashed white boxes are enlarged in the insets and lower images. SypC could also occasionally be seen free in the blood vessels (bv) and in the cytoplasm of the crypt epithelium (white arrows) (*C*). The black timeline indicates at which image locations (*D, E,* and/or *F*) the SypC-carrying hemocytes could be observed when viewed at 9, 12, or 17 hpi. Nuclei were stained with DAPI (blue) and cytoskeleton was labeled with rhodamine phalloidin (yellow). ac, antechamber; cyto, host cytoplasm. (*G*) qRT-PCR determination of the expression level of the C8 subunit of the proteasome. Relative expression of the C8 gene in hemocytes in uncolonized juveniles (Apo) or 24 h postcolonization by either wild-type (WT) or Δ*sypC* symbionts. Differences are indicated by a one-way ANOVA with Tukey's multiple comparison test ($n = 3$). Data are presented as the mean ± 1 SEM. ****$P < 0.0001$.

but it is rare to have trans-Domain functions. While this study of the Syp protein may be the first to describe a bacterial-animal dual-function protein, such proteins have previously been reported between plants and their rhizobial symbionts (48, 49).

Studies of the OMVs have demonstrated that they contain cargo other than SypC that impacts light-organ morphogenesis, such as another outer membrane protein, OmpU (5). In addition, nonprotein cargo of the OMVs influences organ development, including i) MAMPs such as LPS (24) and peptidoglycan derivatives (23, 26) that directly induce the developmental program; and, ii) the small RNA, SsrA (also called tmRNA), which influences host development and symbiont persistence by modulating the host's immune system (17). Several other non-OMV elements are critical for morphogenesis including the symbiont's production of light (22) and modulation of crypt pH (5). The role of the host in this dialogue is similarly complex, coordinating hemocyte migration from the light-organ crypts where OMVs are engulfed, to the blood sinuses of the superficial epithelium where their contents are delivered (Fig. 5). The host responds to this delivery by upregulating expression of genes, such as those encoding the proteasome in the hemocytes as well as metalloproteinases at the base of the developing epithelium. These events enable the normal cell-death process that underlies the morphogenetic program (for review, see ref. 18). Overall, the level of complexity characterizing host–symbiont codevelopment is reminiscent of that evident during embryogenesis: the migration of cells and diffusion of morphogens from one tissue to another, delivering signals and triggering developmental programs. In both progressions, the specification of cell fates is required for a normal, healthy outcome, demanding coordination of several factors both across time and space, and in balanced proportions. The principal difference is that, with a few exceptions (50, 51), embryonic development typically requires coordination only within a single genome; as described here, in a beneficial symbiosis the two

evolutionarily distinct genomes of the bacterium and its host must communicate.

A common feature of animal associations with *Vibrio* species, whether pathogenic or beneficial, may be the functional diversification of SypC, reflected in both the protein's structure and its role in symbiosis. A simulation of SypC using AlphaFold2 (52) suggests the protein may have evolved from another outer membrane transporter, Wza (53), with an increase in domain type (54) and number (*SI Appendix*, Fig. S1). The UniProt database (25) currently lists 14 SypC homologs in conspecifics or congeners of *V. fischeri*. These proteins all have subunits consisting of ~703 amino acids, have similar secondary/tertiary structures, and most have been reported as proteins of mutualistic or pathogenic bacteria of aquatic animals. At the 50+% level of amino acid identity, dozens of proteins are listed, ~2/3 of which are in the Vibrionaceae and have a similar structure, with 700 (±5) amino acids. For example, a SypC homolog has been found in the hydrothermal-vent bacterium, *Vibrio diabolicus* (55). In addition, and relevant here, a *sypC* gene encoding a protein of 699 aa, with 68% sequence identity to *V. fischeri* SypC has been reported as cargo in the OMVs of *Vibrio tasmaniensis*, a pathogen of oysters (56). These phylogenetic patterns of SypC-like proteins suggest a widespread, essential function in host–symbiont interactions of the Vibrionaceae.

The results presented here provide another piece of the puzzle of how a host and its species-specific bacterial symbiont communicate at each new interaction during their 5 My-old partnership. In particular, they address the challenge of how symbiont signals produced deep in the light-organ crypts are transmitted to, and drive host development in, the surface epithelium. The data provide evidence that the transmission is not indirect, i.e., broadcast from the crypt spaces where the symbionts reside by signal transduction cascades passing through the tissues to the surface. Instead, signal delivery appears to be direct, i.e., by the hemocyte-trafficking of OMVs and their cargo to distant tissues that undergo morphogenesis. Many more questions concerning the coordination of this process remain to be addressed. For example: What are the molecular interactions of the SypC protein with the host macrophages that trigger host morphogenesis? Are these interactions direct, or are they indirect, perhaps by affecting the composition or activity of other outer membrane proteins in the OMVs? Do the mechanisms underlying the described behaviors involve the host's immune system or other symbiont MAMPs? Finally, is the structure of the SypC molecule, which appears to be unique to *Vibrio* spp., critical for interactions with the host?

Materials and Methods

Animal Collection and Care. All animal protocols and experiments were approved by the California Institute of Technology Institutional Animal Care and Use Committee. Adult *Euprymna scolopes* Hawaiian bobtail squid were collected from Maunalua Bay, Oahu, HI, and either maintained in flow-through seawater tanks at Kewalo Marine Laboratory (Honolulu, HI) or transferred to recirculating tanks at Caltech (Pasadena, CA) and maintained as previously described (57). Juveniles bred from wild-caught adults were used for all experiments. After embryonic day 10, egg clutches were moved to a natural 12:12-hour light–dark cycle. Upon hatching, juvenile squid were collected, washed, and placed in i) 0.2 μm-pore size filter-sterilized artificial seawater (Instant Ocean, Spectrum Brands, Blacksburg, CA) (FSIO = filter-sterilized Instant Ocean), ii) natural ocean seawater collected from the pier pump of Scripps Institution of Oceanography, La Jolla, CA (SIO seawater), or iii) filter-sterilized ocean seawater (FSOW), as indicated in the figure legends of a given experiment.

Bacterial Strains and Host Colonization Assay. *V. fischeri* strains and plasmids used in this study are listed in *SI Appendix*, Table S1. The ability of different strains to colonize newly hatched juvenile *E. scolopes* was determined as described elsewhere (58, 59) (*SI Appendix*, *Supplemental Methods*).

Imaging of Cell Death in the Appendages. Juvenile squid were collected at 24 h postinoculation, placed in 0.0001% acridine orange (Thermo Fisher Scientific, Irwindale, CA) in FSOW for 1 min, and washed with FSOW. Animals were anesthetized in 2% ethanol and their mantles and funnels were removed to expose the light organ. Light organ appendages were visualized to determine the number of acridine orange positive (early-stage cell death) nuclei using fluorescence confocal microscopy (60) (See *SI Appendix*, Table S2 for details). Late-stage cell death, characterized by DNA fragmentation, was detected by TUNEL staining, according to the manufacturer's instructions (Promega, Madison, WI).

Construction of Protein Fusions in *V. fischeri*. Because an antibody raised to the SypC protein itself was not easily detected by ICC, N-terminal mCherry translational fusions were constructed by amplification of *mCherry* from pSMV3-*mCherry-zapA* (61) and either *sypC* or *ompU* from the *V. fischeri* ES114 genome by standard Gibson assembly into pVSV105 (62). All fusions include an internal linker sequence (5′-CTCGAGGGATCCGGA-3′) between *mCherry* and the gene of interest (See *SI Appendix*, Table S1). pCMC37 was cloned with the native signal peptide sequence of *ompU* on the 5′ end of the fusion sequence. Transfer of plasmids into *V. fischeri* strains was performed by standard biparental conjugation protocol (63) using the *E. coli* donor strain MFDpir (64).

Immunocytochemistry of SypC and OmpU. Juvenile squid were colonized within 3 h of hatching, at 1 h postdusk with 10,000 CFU of bacteria per ml (either WT+ mCherry, WT + mCherry-SypC conjugate, or WT + mCherry-OmpU conjugate). Colonization was confirmed via luminometer prior to fixation. Squid were fixed at 4 and 10 h postdawn (15 and 21 h postcolonization) in 4% PFA in marine PBS (mPBS) for 12 h at 4 °C with agitation, then rinsed four times for 15 min in mPBS. Light organs were dissected out of the squid and permeabilized for two days in mPBS/1% Triton X-100 (mPBST) at 4 °C with agitation. Blocking solution (0.5% BSA, 1% goat serum in mPBST) was added and samples were incubated in the dark overnight at 4 °C with agitation. Either an anti-mCherry monoclonal antibody (Thermo Fisher Scientific) or the corresponding rat IgG isotype control (Thermo Fisher Scientific) was added at a concentration of 1:100 in blocking solution and incubated in the dark for 14 d at 4 °C with agitation; fresh antibody was replaced at 7 d. Samples were rinsed 4 × 1 h with mPBST and goat anti-rat IgG secondary antibody (Alexa Fluor 647 conjugated, Thermo Fisher Scientific) was added at 1:1000 concentration in blocking solution overnight. Samples were rinsed 5 × 5 min in mPBST, and 1 × 5 min in 5× SSCT, then counterstained with 1:1,000 CellMask Orange Plasma Membrane Stain, and 1:50 DAPI (Thermo Fisher Scientific), in mPBST for two days at 4 °C with agitation.

Light organs were mounted in Vectashield (Fisher Scientific, Hampton, NH) on slides for confocal microscopy imaging. Lasers were set to the negative control to eliminate background autofluorescence and identical imaging parameters were used across all samples. Specific confocal microscope and imaging acquisition parameters are listed in *SI Appendix*, Table S2. Three-dimensional reconstructions of 0.3 μm thick Z-stacks were generated using Imaris 10.1 (Bitplane, Zurich, Switzerland).

Electron Tomography. Samples of the light organ were prepared for electron microscopy. For sample preparation and details of the electron tomography and scanning electron microscopy methods, see *SI Appendix*, Table S2 and *Supplemental Methods*.

TCT Production by *V. fischeri*. Analyses of the production of this MAMP by cultures of *V. fischeri* have been reported elsewhere and can be found in *SI Appendix*, *Supplemental Methods*.

OMV Isolation. OMVs were isolated from *V. fischeri* cultures after 24 h of growth in LBS at 28 °C as previously described (5) (see *SI Appendix*, *Supplemental Methods* for details).

RNA Extraction for RNAseq and NanoString Experiments. Juvenile squid were hatched into *V. fischeri*-free natural ocean water. Animals hatched on the same day and from the same clutch (i.e., with a related genetic background) were separated into 3 treatments groups: APO (no exposure to *V. fischeri*), WT (exposed to wild-type *V. fischeri* strain ES114 at ~5,000 CFU/mL), and Δ*sypC* (exposed to a *V. fischeri* Δ*sypC* derivative at ~5,000 CFU/mL); n = 20 animals per sample, with 4 biological replicates. After 24 h of exposure, total light-organ RNA was isolated using an RNeasy Mini Kit (Qiagen, Germantown, MD) and Qiagen QIAshredder according to the manufacturer's instructions. Samples were treated with TURBO

DNase (Thermo Fisher Scientific) to remove DNA contamination. RNA quality and concentration were determined by spectrophotometry using a NanoPhotometer (Implen, Westlake City, CA), and the concentration was confirmed using Qubit RNA BR assay kit (Thermo Fisher Scientific). For RNAseq analysis, the Illumina TruSeq Stranded mRNA Sample Prep with polyA selection v4.0 protocol was used for library preparation. Sequencing of light-organ tissue samples was performed at the NYU Genome Center on an Illumina HiSeq 4000 using a paired-end, 100-nucleotide-length run mode that produced ~35 to 85 million reads/sample.

For NanoString codeset analysis, RNA was prepared from APO, WT, and Δ*sypC* animals as described above. Raw nCounter data were passed into Rs NanoStringDiff (v1), which computed $\log_2$FC and qvalue to identify differentially expressed genes (DEGs); two host genes, serine hydroxymethyltransferase and REL_NF-kappaB, were chosen for normalization. Clutch number (as a proxy for genetic background) was included as a covariate in the model. nSolver (v4.0) was used to normalize raw NanoString data for visualization.

Determination of Differential Gene Expression. Raw PE reads were quality- and adapter-trimmed using fastp (v0.24.0) with default parameters (65). Cleaned reads where then pseudoaligned, to the most recently published *E. scolopes* reference genome and annotations (v2.2) (66), using kb-python with bulk RNA-seq and reverse stranded tags (kb-python: v0.28.2, kallisto v0.50.0, bustools: v0.43.2) (67). On average, 64.4% of reads successfully pseudoaligned. Gene-level counts were then passed into R's DESeq2 (v1.44.0) for differential expression analysis (68). Genetic background, or clutch, was included as a covariate in the model. DEG were identified for each pairwise comparison, due to high within sample variation, with *P*-value adjusted globally (DE: global padj <0.05, log2FC ± 0.5). Plots were made with ggplot2 (v3.5.1), ComplexUpsetR (v1.3.3), and variancePartition (v1.34.0).

Statistical Analyses. All statistical analyses were conducted using Prism 8 (Graphpad Software, La Jolla, CA). Statistical analyses between two groups were analyzed using unpaired Student's *t* test. Comparisons between multiple groups were analyzed using two-way ANOVA with Tukey test. Statistical variability is expressed as mean ± 1 SD; ns: not significant, $P > 0.05$; *$P \leq 0.05$; **$P \leq 0.01$; ***$P \leq 0.001$; ****$P \leq 0.0001$. N values for experiments are indicated in figure legends as appropriate.

Data, Materials, and Software Availability. The data supporting the findings of this study are available within the article and its *SI Appendix*. The transcriptomic raw sequencing data generated in this study have been deposited in Gene Expression Omnibus under accession numbers GSE307160 (69) and GPL36208 (70). Relevant code for this manuscript is available at https://github.com/verabeil/escolopes_vfischeri_sypc.git (71).

ACKNOWLEDGMENTS. We thank Zachary A. Yahiku and Hannah Osland for their technical help. Dr. William Goldman (University of North Carolina at Chapel Hill) provided purified TCT. Dr. Joram Piatigorsky provided valuable advice. This work was supported by funding from the NIH Grants R37-AI50661 to M.M.-N. and E.G.R. and R01-GM135254 to E.G.R. and M.M.-N.

Author affiliations: [a]Pacific Biosciences Research Center, Kewalo Marine Laboratory, University of Hawaii at Manoa, Honolulu, HI 96813; [b]Division of Biosphere Sciences and Engineering, Carnegie Science, Pasadena, CA 91125; [c]Division of Biology and Biological Engineering, California Institute of Technology, Pasadena, CA 91125; [d]Department of Medical Microbiology and Immunology, University of Wisconsin-Madison, School of Medicine and Public Health, Madison, WI 53705; and [e]Department of Microbiology and Immunology, Loyola University Medical Center, Maywood, IL 60153

1. V. Tiku, M. W. Tan, Host immunity and cellular responses to bacterial outer membrane vesicles. *Trends Immunol.* **42**, 1024–1036 (2021).
2. M. Toyofuku, S. Schild, M. Kaparakis-Liaskos, L. Eberl, Composition and functions of bacterial membrane vesicles. *Nat. Rev. Microbiol.* **21**, 415–430 (2023).
3. L. Turnbull *et al.*, Explosive cell lysis as a mechanism for the biogenesis of bacterial membrane vesicles and biofilms. *Nat. Commun.* **7**, 11220 (2016).
4. L. Zavan *et al.*, The mechanism of *Pseudomonas aeruginosa* outer membrane vesicle biogenesis determines their protein composition. *Proteomics* **23**, e2200464 (2023).
5. J. B. Lynch *et al.*, Ambient pH alters the protein content of outer membrane vesicles, driving host development in a beneficial symbiosis. *J. Bacteriol.* **201**, e00319-19 (2019).
6. M. G. Sartorio, E. J. Pardue, N. E. Scott, M. F. Feldman, Human gut bacteria tailor extracellular vesicle cargo for the breakdown of diet- and host-derived glycans. *Proc. Natl. Acad. Sci. U.S.A.* **120**, e2306314120 (2023).
7. S. K. Cohen *et al.*, Tracking the cargo of extracellular symbionts into host tissues with correlated electron microscopy and nanoscale secondary ion mass spectrometry imaging. *Cell Microbiol.* **22**, e13177 (2020).
8. D. N. Villageliu, D. R. Samuelson, The role of bacterial membrane vesicles in human health and disease. *Front. Microbiol.* **13**, 828704 (2022).
9. F. S. Abolhasani *et al.*, Outer membrane vesicles in gram-negative bacteria and its correlation with pathogenesis. *Front. Immunol.* **16**, 1541636 (2025).
10. J. Li *et al.*, Outer membrane vesicles produced by coral-associated *Vibrio coralliilyticus* inhibit bacteriophage infection and its ecological implications. *Microbiol. Res.* **281**, 127607 (2024).
11. H. Gao *et al.*, Outer membrane vesicles from a mosquito commensal mediate targeted killing of *Plasmodium* parasites via the phosphatidylcholine scavenging pathway. *Nat. Commun.* **14**, 5157 (2023).
12. J. B. Lynch, R. A. Alegado, Spheres of hope, packets of doom: The good and bad of outer membrane vesicles in interspecies and ecological dynamics. *J. Bacteriol.* **199**, e00012-17 (2017).
13. G. Wu *et al.*, Outer membrane vesicles induce the mussel plantigrade settlement via regulation of c-di-GMP. *Biofouling* **39**, 359–370 (2023).
14. Y. Shen *et al.*, Outer membrane vesicles of a human commensal mediate immune regulation and disease protection. *Cell Host Microbe* **12**, 509–520 (2012).
15. A. Kaisanlahti *et al.*, Bacterial extracellular vesicles - brain invaders? A systematic review. *Front. Mol. Neurosci.* **16**, 1227655 (2023).
16. M. S. Aschtgen *et al.*, Rotation of *Vibrio fischeri* flagella produces outer membrane vesicles that induce host development. *J. Bacteriol.* **198**, 2156–2165 (2016).
17. S. Moriano-Gutierrez *et al.*, The noncoding small RNA SsrA is released by *Vibrio fischeri* and modulates critical host responses. *PLoS Biol.* **18**, e3000934 (2020).
18. S. V. Nyholm, M. J. McFall-Ngai, A lasting symbiosis: How the Hawaiian bobtail squid finds and keeps its bioluminescent bacterial partner. *Nat. Rev. Microbiol.* **19**, 666–679 (2021).
19. K. L. Visick, E. V. Stabb, E. G. Ruby, A lasting symbiosis: How *Vibrio fischeri* finds a squid partner and persists within its natural host. *Nat. Rev. Microbiol.* **19**, 654–665 (2021).
20. B. L. Fung, J. J. Esin, K. L. Visick, *Vibrio fischeri*: A model for host-associated biofilm formation. *J. Bacteriol.* **206**, e0037023 (2024).
21. T. Koropatnick, M. S. Goodson, E. A. Heath-Heckman, M. McFall-Ngai, Identifying the cellular mechanisms of symbiont-induced epithelial morphogenesis in the squid- association. *Biol. Bull.* **226**, 56–68 (2014).
22. M. McFall-Ngai, E. A. Heath-Heckman, A. A. Gillette, S. M. Peyer, E. A. Harvie, The secret languages of coevolved symbioses: Insights from the *Euprymna scolopes*-*Vibrio fischeri* symbiosis. *Semin. Immunol.* **24**, 3–8 (2012).
23. M. S. Aschtgen, K. Wetzel, W. Goldman, M. McFall-Ngai, E. Ruby, *Vibrio fischeri*-derived outer membrane vesicles trigger host development. *Cell Microbiol.* **18**, 488–499 (2016).
24. J. S. Foster, M. A. Apicella, M. J. McFall-Ngai, *Vibrio fischeri* lipopolysaccharide induces developmental apoptosis, but not complete morphogenesis, of the *Euprymna scolopes* symbiotic light organ. *Dev. Biol.* **226**, 242–254 (2000).
25. C. UniProt, UniProt: The universal protein knowledgebase in 2025. *Nucleic Acids Res.* **53**, D609–D617 (2025).
26. T. A. Koropatnick *et al.*, Microbial factor-mediated development in a host-bacterial mutualism. *Science* **306**, 1186–1188 (2004).
27. E. S. Yip, B. T. Grublesky, E. A. Hussa, K. L. Visick, A novel, conserved cluster of genes promotes symbiotic colonization and sigma-dependent biofilm formation by *Vibrio fischeri*. *Mol. Microbiol.* **57**, 1485–1498 (2005).
28. S. Shibata, E. S. Yip, K. P. Quirke, J. M. Ondrey, K. L. Visick, Roles of the structural symbiosis polysaccharide (syp) genes in host colonization, biofilm formation, and polysaccharide biosynthesis in *Vibrio fischeri*. *J. Bacteriol.* **194**, 6736–6747 (2012).
29. T. A. Koropatnick, M. S. Goodson, E. A. Heath-Heckman, M. McFall-Ngai, Identifying the cellular mechanisms of symbiont-induced epithelial morphogenesis in the squid-vibrio association. *Biol. Bull.* **226**, 56–68 (2014).
30. Y. Hong, M. A. Liu, P. R. Reeves, Progress in our understanding of Wzx flippase for translocation of bacterial membrane lipid-linked oligosaccharide. *J. Bacteriol.* **200**, e00154-17 (2018).
31. J. A. Doino, M. J. McFall-Ngai, A transient exposure to symbiosis-competent bacteria induces light organ morphogenesis in the host squid. *Biol. Bull.* **189**, 347–355 (1995).
32. T. Essock-Burns, C. Bongrand, W. E. Goldman, E. G. Ruby, M. J. McFall-Ngai, Interactions of symbiotic partners drive the development of a complex biogeography in the squid–vibrio symbiosis. *mBio* **11**, e00853-20 (2020).
33. L. K. Sycuro, E. G. Ruby, M. McFall-Ngai, Confocal microscopy of the light organ crypts in juvenile *Euprymna scolopes* reveals their morphological complexity and dynamic function in symbiosis. *J. Morphol.* **267**, 555–568 (2006).
34. T. A. Koropatnick, J. R. Kimbell, M. J. McFall-Ngai, Responses of host hemocytes during the initiation of the squid-vibrio symbiosis. *Biol. Bull.* **212**, 29–39 (2007).
35. J. R. Kimbell, T. A. Koropatnick, M. J. McFall-Ngai, Evidence for the participation of the proteasome in symbiont-induced tissue morphogenesis. *Biol. Bull.* **211**, 1–6 (2006).
36. K. E. Zink *et al.*, A small molecule coordinates symbiotic behaviors in a host organ. *mBio* **12**, e03637-20 (2021).
37. S. Moriano-Gutierrez *et al.*, Critical symbiont signals drive both local and systemic changes in diel and developmental host gene expression. *Proc. Natl. Acad. Sci. U.S.A.* **116**, 7990–7999 (2019).
38. J. D. Cecil, N. Sirisaengtaksin, N. M. O'Brien-Simpson, A. M. Krachler, Outer membrane vesicle-host cell interactions. *Microbiol. Spectr.* **7**, 7.1.06 (2019).
39. J. M. Bomberger *et al.*, Long-distance delivery of bacterial virulence factors by *Pseudomonas aeruginosa* outer membrane vesicles. *PLoS Pathog.* **5**, e1000382 (2009).
40. K. Wang, C. Jia, B. Zhang, J. Chen, J. Zhao, Outer membrane vesicles from commensal microbes contribute to the sponge *Tedania* sp. development by regulating the expression level of apoptosis-inducing factor (AIF). *Commun. Biol.* **7**, 952 (2024).
41. A. Woznica *et al.*, Bacterial lipids activate, synergize, and inhibit a developmental switch in choanoflagellates. *Proc. Natl. Acad. Sci. U.S.A.* **113**, 7894–7899 (2016).
42. S. Chen, Q. Lei, X. Zou, D. Ma, The role and mechanisms of gram-negative bacterial outer membrane vesicles in inflammatory diseases. *Front. Immunol.* **14**, 1157813 (2023).
43. R. Stentz, A. L. Carvalho, E. J. Jones, S. R. Carding, Fantastic voyage: The journey of intestinal microbiota-derived microvesicles through the body. *Biochem. Soc. Trans.* **46**, 1021–1027 (2018).

44. A. Kaisanlahti *et al.*, Maternal microbiota communicates with the fetus through microbiota-derived extracellular vesicles. *Microbiome* **11**, 249 (2023).
45. M. S. Aschtgen *et al.*, Insights into flagellar function and mechanism from the squid-*Vibrio* symbiosis. *NPJ Biofilms Microbiomes* **5**, 32 (2019).
46. S. Dhital, P. Deo, I. Stuart, T. Naderer, Bacterial outer membrane vesicles and host cell death signaling. *Trends Microbiol.* **29**, 1106–1116 (2021).
47. B. M. Coffey, S. S. Akhand, G. G. Anderson, MgtE is a dual-function protein in *Pseudomonas aeruginosa*. *Microbiology (Reading, Engl.).* **160**, 1200–1213 (2014).
48. D. Liu, A. K. Bhunia, Anchorless bacterial moonlighting metabolic enzymes modulate the immune system and contribute to pathogenesis. *ACS Infect. Dis.* **10**, 2551–2566 (2024).
49. F. Sorroche *et al.*, The *ex planta* signal activity of a *Medicago* ribosomal uL2 protein suggests a moonlighting role in controlling secondary rhizobial infection. *PLoS One* **15**, e0235446 (2020).
50. K. E. Malter *et al.*, A bacterial membrane-disrupting protein stimulates animal metamorphosis. *mBio* **16**, e0357324 (2025).
51. B. Qi, M. Han, Microbial siderophore enterobactin promotes mitochondrial ion uptake and development of the host via interaction with ATP synthase. *Cell* **175**, 571–582.e511 (2018).
52. J. Jumper *et al.*, Highly accurate protein structure prediction with AlphaFold. *Nature* **596**, 583–589 (2021).
53. R. F. Collins, J. P. Derrick, Wza: A new structural paradigm for outer membrane secretory proteins?. *Trends Microbiol.* **15**, 96–100 (2007).
54. A. M. Burroughs, S. Balaji, L. M. Iyer, L. Aravind, A novel superfamily containing the beta-grasp fold involved in binding diverse soluble ligands. *Biol. Direct* **2**, 4 (2007).
55. D. Goudenege *et al.*, Genome sequence of *Vibrio diabolicus* and identification of the exopolysaccharide HE800 biosynthesis locus. *Appl. Microbiol. Biotechnol.* **98**, 10165–10176 (2014).
56. A. S. Vanhove *et al.*, Outer membrane vesicles are vehicles for the delivery of *Vibrio tasmaniensis* virulence factors to oyster immune cells. *Environ. Microbiol.* **17**, 1152–1165 (2015).
57. A. C. Hargadon *et al.*, An acidic microenvironment produced by the V-type ATPase of *Euprymna scolopes* promotes specificity during *Vibrio fischeri* recruitment. *Commun. Biol.* **7**, 1642 (2024).
58. E. J. Koch, T. Miyashiro, M. J. McFall-Ngai, E. G. Ruby, Features governing symbiont persistence in the squid-vibrio association. *Mol. Ecol.* **23**, 1624–1634 (2014).
59. L. M. Naughton, M. J. Mandel, Colonization of *Euprymna scolopes* squid by *Vibrio fischeri*. *J. Vis. Exp.* **10**, e3758 (2012).
60. M. K. Montgomery, M. McFall-Ngai, Bacterial symbionts induce host organ morphogenesis during early postembryonic development of the squid *Euprymna scolopes*. *Development* **120**, 1719–1729 (1994).
61. L. Yang *et al.*, Bacterial growth dynamics in a rhythmic symbiosis. *Mol. Biol. Cell* **35**, ar79 (2024).
62. A. K. Dunn, D. S. Millikan, D. M. Adin, J. L. Bose, E. V. Stabb, New rfp- and pES213-derived tools for analyzing symbiotic *Vibrio fischeri* reveal patterns of infection and *lux* expression in situ. *Appl. Environ. Microbiol.* **72**, 802–810 (2006).
63. K. L. Visick, K. M. Hodge-Hanson, A. H. Tischler, A. K. Bennett, V. Mastrodomenico, Tools for rapid genetic engineering of *Vibrio fischeri*. *Appl. Environ. Microbiol.* **84**, e00850-18 (2018).
64. L. Ferrieres *et al.*, Silent mischief: Bacteriophage Mu insertions contaminate products of *Escherichia coli* random mutagenesis performed using suicidal transposon delivery plasmids mobilized by broad-host-range RP4 conjugative machinery. *J. Bacteriol.* **192**, 6418–6427 (2010).
65. S. Chen, Ultrafast one-pass FASTQ data preprocessing, quality control, and deduplication using fastp. *Imeta* **2**, e107 (2023).
66. T. F. Rogers *et al.*, Gene modelling and annotation for the Hawaiian bobtail squid. *Euprymna scolopes*. *Sci. Data* **11**, 40 (2024).
67. P. Melsted *et al.*, Modular, efficient and constant-memory single-cell RNA-seq preprocessing. *Nat. Biotechnol.* **39**, 813–818 (2021).
68. M. I. Love, W. Huber, S. Anders, Moderated estimation of fold change and dispersion for RNA-seq data with DESeq2. *Genome Biol.* **15**, 550 (2014).
69. J. T. Kuwabara, V. Beilinson, Data from "SypC, a symbiont outer membrane vesicle protein, impacts the development of the squid-vibrio partnership". Gene Expression Omnibus. https://www.ncbi.nlm.nih.gov/geo/query/acc.cgi?acc=GSE307160. Deposited 3 September 2025.
70. J. T. Kuwabara, V. Beilinson, E.G. Ruby, Data from "SypC, a symbiont outer membrane vesicle protein, impacts the development of the squid-vibrio partnership". Gene Expression Omnibus. https://www.ncbi.nlm.nih.gov/geo/query/acc.cgi?acc=GPL36208. Deposited 3 September 2025.
71. V. Beilinson, Data from "SypC, a symbiont outer membrane vesicle protein, impacts the development of the squid-vibrio partnership". GitHub. https://github.com/verabeil/escolopes_vfischeri_sypc. Deposited 25 February 2026.

PNAS

Supporting Information for

SypC, a Symbiont Outer-Membrane-Vesicle Protein, Impacts the Development and Persistence of the Squid-Vibrio Partnership

Jill T. Kuwabara, Vera Beilinson, Alexis C. Hargadon, Grischa Y. Chen, Xiao-Meng Hu, Mark S. Ladinsky, Kathleen T. Hackett, Joseph R. Dillard, Karen L. Visick, Edward G. Ruby, Margaret McFall-Ngai

Margaret McFall-Ngai
Email: mcfallng@caltech.edu

This PDF file includes:

Supporting Information Text

SUPPLEMENTAL METHODS

Bacterial strains and media

V. fischeri strain ES114 was used as the wild-type strain, and as the parent strain for a number of mutants (See SI Appendix, table S1). To prepare an inoculum for light-organ colonization experiments (1), strains were cultured overnight in Luria-Bertani salt medium (LBS) (2). To maintain plasmid constructs, chloramphenicol (Cm) was added to LBS at a concentration of 2.5 mg/ml. The strains were then subcultured (1:100) into seawater tryptone medium (SWT) (3) and grown to mid-log phase at 28 °C with shaking. The SWT culture was diluted into seawater to a final concentration of between 0.5 and 1 x 10^4 CFU/ml to serve as an inoculum for the newly hatched juvenile squid.

Construction of protein fusions in *V. fischeri*

Briefly, N-terminal *mCherry* translational fusions were constructed by amplification of mCherry from pSMV3-*mCherry-zapA* (4) and either the *sypC* or *ompU* gene from the *V. fischeri* ES114 genome by standard Gibson assembly into pVSV105 (5). All fusions include an internal linker sequence (5'-CTCGAGGGATCCGGA-3') between *mCherry* and the gene of interest. pCMC37 (See SI Appendix, table S1) were cloned with the native signal peptide sequence of *ompU* and *sypC*, respectively, on the 5' end of the fusion sequence. Transfer of plasmids into *V. fischeri* strains was performed by a standard biparental conjugation protocol (6) using the *E. coli* donor strain MFDpir (7).

Host colonization assay

Within 2 h of hatching, juvenile squid were colonized by overnight exposure to *V. fischeri* cells or kept aposymbiotic (APO, *i.e.*, exposed only to the ~10^6 non-specific bacteria per ml in the

bacterioplankton), or in filter-sterilized Instant Ocean (Instant Ocean, Spectrum Brands, Blacksburg, CA) (FSIO). Colonization was monitored by checking luminescence of the animal with a TD-20/20 luminometer (Turner Designs, San Jose, CA). The number of colony-forming units (CFU) in the light organ of squid was determined by plating dilutions of homogenized light-organ contents on LBS plates as previously described (4). Relative light units (RLU) were determined by normalizing the luminescence reading by the number of CFU in each individual light organ.

TCT production by *V. fischeri*

To determine the amount of peptidoglycan monomer (tracheal cytotoxin; TCT) exported from wild-type and Δ*sypC* mutant cells, peptidoglycan (PG) fragments were purified from (90 mL) of *V. fischeri* supernatant. For binding the PG from the supernatant, 6-mL C18 SepPak cartridges (Waters Corp., Milford, MA) were prepared by washing the cartridges with 6 mL methanol, followed by two washes with 6 mL 0.1% trifluoroacetic acid (TFA). TFA was added to the culture supernatant sample to a final concentration of 0.1%. The sample was loaded on the cartridge, and the volume of liquid was slowly pulled through the cartridge using a syringe on a short length of tubing attached to the bottom of the cartridge. The cartridge was washed twice with 6 mL 0.1% TFA. PG fragments were eluted from the cartridge with 3 mL methanol. The samples were evaporated under vacuum, and each was suspended in 50 µL of LC/MS grade H_2O.

The samples were analyzed by UPLC/MS (ultra-performance liquid chromatography/mass spectrometry) using a Waters Acquity UPLC CSH C18 column, 1.7 µm particle size, 2.1 x 150 mm using a flow rate of 0.5 mL/min. A volume of 10 µL of the sample was injected, and the column temperature was maintained at 40 ˚C. Separation was achieved using a linear gradient

spread over 5 min of 2-15% acetonitrile in 2% formic acid. Absorbance was measured at 206 nm and 254 nm. Mass spectrometry was performed in the positive electrospray ionization mode (ESI^+) with the capillary voltage at 0.8 kV and the cone voltage at 15.

Imaging of squid light organs

Juvenile squid were fixed in 4% paraformaldehyde (PFA) in marine phosphate-buffered saline (mPBS; 50 mM sodium phosphate buffer, 450 mM NaCl, pH 7.4) overnight at 4 °C, then washed three times for 30 min in mPBS. Staining was performed on dissected light organ tissue; CellMask Orange Plasma Membrane Stain (Thermo Fischer Scientific, Irwindale, CA) highlights the lipid-rich vesicles within cells. To visualize hemocytes, light organs were stained with deoxyribonuclease 1/Alexa Fluor 488 conjugate (DNase-1) (Thermo Fisher Scientific) in 1% Triton X-100 in mPBS (mPBST) for 24 h, at 4 °C. To visualize late-stage cell death (characterized by DNA fragmentation), light organs were stained with TUNEL according to the manufacturer's protocol (Promega, Madison, WI). Light organs were counterstained overnight with either DAPI or TO-PRO-3 (Thermo Fisher Scientific) to visualize host nuclei, and phalloidin (Invitrogen, Carlsbad, CA) to visualize host actin cytoskeleton and the host cell boundary. Samples were mounted on slides with Vectashield (Vector Laboratories, Newark, CA) and imaging was performed on an upright Zeiss LSM 980 laser-scanning confocal microscope (LSCM) at Caltech, a Zeiss LSM 710 at Kewalo Marine Laboratory, or an inverted Zeiss LSM 800 LSCM at the Caltech Biological Imaging Facility (See SI Appendix, table S2). Images and figures were edited in either Photoshop CS6 (Adobe) or Fiji (ImageJ).

Sample preparation for electron microscopy

Squid light organs were dissected from the animal body cavity and immediately pre-fixed with 3% glutaraldehyde, 1% paraformaldehyde, 5% sucrose in marine PBS. Whole light organs were

rinsed with fresh mPBS containing 10% Ficoll (Sigma-Aldrich, St. Louis, MO), placed into brass planchettes (Ted Pella, Inc., Redding, CA) and rapidly frozen with a Wohlwend Compact-03 high pressure freezer (Technotrade International Inc., Manchester, NH). The vitrified samples were transferred under liquid nitrogen to cryotubes (Nunc) containing a frozen solution of 2.5% osmium tetroxide and 0.05% uranyl acetate in acetone. Tubes were loaded into an AFS-2 freeze-substitution machine (Leica Microsystems, Wetzlar, Germany) and processed at -90 °C for 72 h, warmed over 12 h to -20 °C, held at that temperature for 6 h, then warmed to 4 °C for 2 h. Fixative was removed and samples were rinsed 4-times with cold acetone, then infiltrated with Epon-Araldite resin (Electron Microscopy Sciences, Hatfield, PA) over 48 h. Samples were flat-embedded between two Teflon-coated glass microscope slides and resin polymerized at 60 °C for 48 h.

Embedded light organs were viewed by phase-contrast microscopy to identify optimal specimens. These were excised with a #11 scalpel and glued to the tips of plastic sectioning stubs. Semi-thin (170 nm) serial sections were cut with an EM UC6 ultramicrotome (Leica Microsystems) using a diamond knife (Diatome, Ltd., Bern, Switzerland). Sections were transferred to Formvar-coated copper-rhodium 1-mm slot grids (Electron Microscopy Sciences, Port Washington, PA) and stained with uranyl acetate and lead citrate. Gold beads (10 nm) were placed on both surfaces of the grids to serve as fiducial markers for tomographic image alignment.

Electron tomography

Grids were placed in a Model 2040 dual-axis tomography holder (E.A. Fischione Instruments, Export, PA) and imaged with a Tecnai T12-G2 transmission electron microscope (120 KeV, Thermo Fisher Scientific) equipped with a XP1000 2k x 2k CCD camera (Gatan, Inc.

Pleasanton, CA). Tomographic tilt-series and large-area montaged overviews were acquired automatically using the SerialEM software package (8). For tomography, samples were tilted ±62° and images collected at 1° intervals. The grid was then rotated 90° and a similar series taken about the orthogonal axis. Tomographic data was calculated, analyzed, and modeled using the IMOD software package (8-10) on iMac Pro and Mac Studio M1 computers (Apple, Inc.).

Scanning electron microscopy

Tissue was fixed with 4% PFA in mPBS for 24 h, post-fixed with 1% osmium tetroxide in 0.1 M sodium cacodylate, dehydrated through an ethanol series, and dried in a Tousimis Samdri-795 critical point dryer. Samples were mounted on aluminum stubs with double-stick carbon tape and coated with gold/palladium in a Hummer 6.2 sputter coater. Samples were viewed and digital images were acquired with a Hitachi S-4800 field emission scanning electron microscope at an accelerating voltage of 5 kV.

Outer membrane vesicle (OMV) purification

Single-membrane OMVs were isolated from *V. fischeri* cultures after 24 h of growth in LBS at 28 °C as previously described, and contained almost entirely outer-membrane embedded (*e.g.*, SypC) and periplasmic proteins (11). Briefly, the cells were pelleted at 8,000 x g at 4 °C for 10 min. The culture supernatant was filtered through a 0.22-µm polyethersulfone membrane filter to remove any contaminating cells. OMVs were then collected from the filtered supernatant by centrifugation at 173,000 x g for 2 h at 4 °C using a Type 45 Ti rotor in an Optima XE-90 ultracentrifuge (Beckman Coulter, Brea, CA). Pellets containing OMVs were resuspended in Dulbecco's phosphate-buffered saline supplemented with NaCl (dPBS-NaCl: 422 mM NaCl, 2.7 mM KCl, 1.5 mM KH_2PO4, 7.7 mM Na_2HPO_4, 900 M $CaCl_2$, 500 M $MgCl_2$). OMVs were further purified with a discontinuous density gradient (sucrose layers of 25, 35, 40, 45, 50, and

55%, wt/vol) and centrifugation at 90,000 x g for 15 h at 4 °C using an MLA-50 rotor in an Optima MAX-XP ultracentrifuge (Beckman Coulter). The OMVs were pelleted at 173,000 g and 4°C for 4 h and resuspended in dPBS-NaCl. The total OMV protein concentration was measured using a Qubit 2.0 Fluorometer (Thermo Fisher). Samples were diluted to equal concentrations with dPBS-NaCl before addition to FSIO for squid exposure experiments. Squid were treated with 100 mg of OMV proteins per ml for 18 h.

RNA extraction and qRT-PCR analysis

Hemocytes were isolated from both aposymbiotic and colonized juvenile squids as previously described (12). The isolated hemocyte samples were treated with RNAlater (Invitrogen) for 1 h, and total RNA was extracted using the RNeasy Mini Kit (Qiagen, Germantown, MD). Genomic DNA contamination was removed by treatment with TURBO DNase (Thermo Fisher Scientific). The integrity and quality of the RNA were assessed by agarose gel electrophoresis and NanoDrop spectrophotometry (Thermo Fisher Scientific). RNA concentration was quantified using the high-sensitivity Qubit RNA HS Assay Kit (Invitrogen). For each sample, 50 ng of RNA was reverse-transcribed into cDNA using the LunaScript RT SuperMix Kit (New England Biolabs, Ipswich, MA) in a 20 μL reaction.

Primers for the C8 subunit of proteasome gene were designed using Primer 5.00 (PREMIER Biosoft International, San Francisco, CA), and primers for the 40S gene, serving as the endogenous reference were adopted from (13). Selected primer pairs showed single melting peaks and acceptable amplification performance. The expression of 40S gene was stable across all samples in this experiment. Quantitative real-time PCR was performed using SsoAdvanced Universal SYBR Green Supermix (Bio-Rad, Hercules) on a QuantStudio 5 system (Applied

Biosystems, Foster City, CA). Relative gene expression levels of C8 subunit of proteasome gene were calculated using the $2^{-\Delta\Delta Ct}$ method (14).

SUPPLEMENTAL RESULTS

PERMANOVA analyses of RNAseq data

PERMANOVA indicated significant global differences among conditions ($R^2 = 0.31$, $p = 0.012$). Pairwise PERMANOVA showed that APO differed from both WT ($R^2 = 0.35$, adj. $p = 0.0495$) and Δ*sypC* ($R^2 = 0.26$, adj. $p = 0.0495$), whereas WT and Δ*sypC* were not significantly different ($R^2 = 0.11$, $p = 0.72$). Pairwise tests for homogeneity of multivariate dispersion were non-significant (all $p > 0.10$), confirming that these results are not driven by unequal dispersion. Importantly, the lack of global separation between WT and Δ*sypC* did not invalidate the differential expression results. Instead, it indicated that Δ*sypC* colonization does not broadly reprogram host transcription, but produces focused, pathway-specific changes—consistent with the PCA, where WT and Δ*sypC* clustered tightly together and apart from APO. The lack of PERMANOVA significance between WT and Δ*sypC* likely reflected high biological variability relative to the scale of transcriptional differences between these groups. This pattern underscored that the presence of bacteria was the dominant driver of host transcriptional state, whereas the loss of a single bacterial gene (Δ*sypC*) led to more targeted effects. To resolve these subtler differences, we implemented a tiered DEG framework (brown, yellow, and green categories). Within this system, the "green" DEGs represent the strongest candidates (Fig. 2*B* and *C*), as they were not differentially expressed between APO and Δ*sypC*, but were distinct in WT, suggesting that these genes are specifically dependent on SypC activity rather than general colonization status.

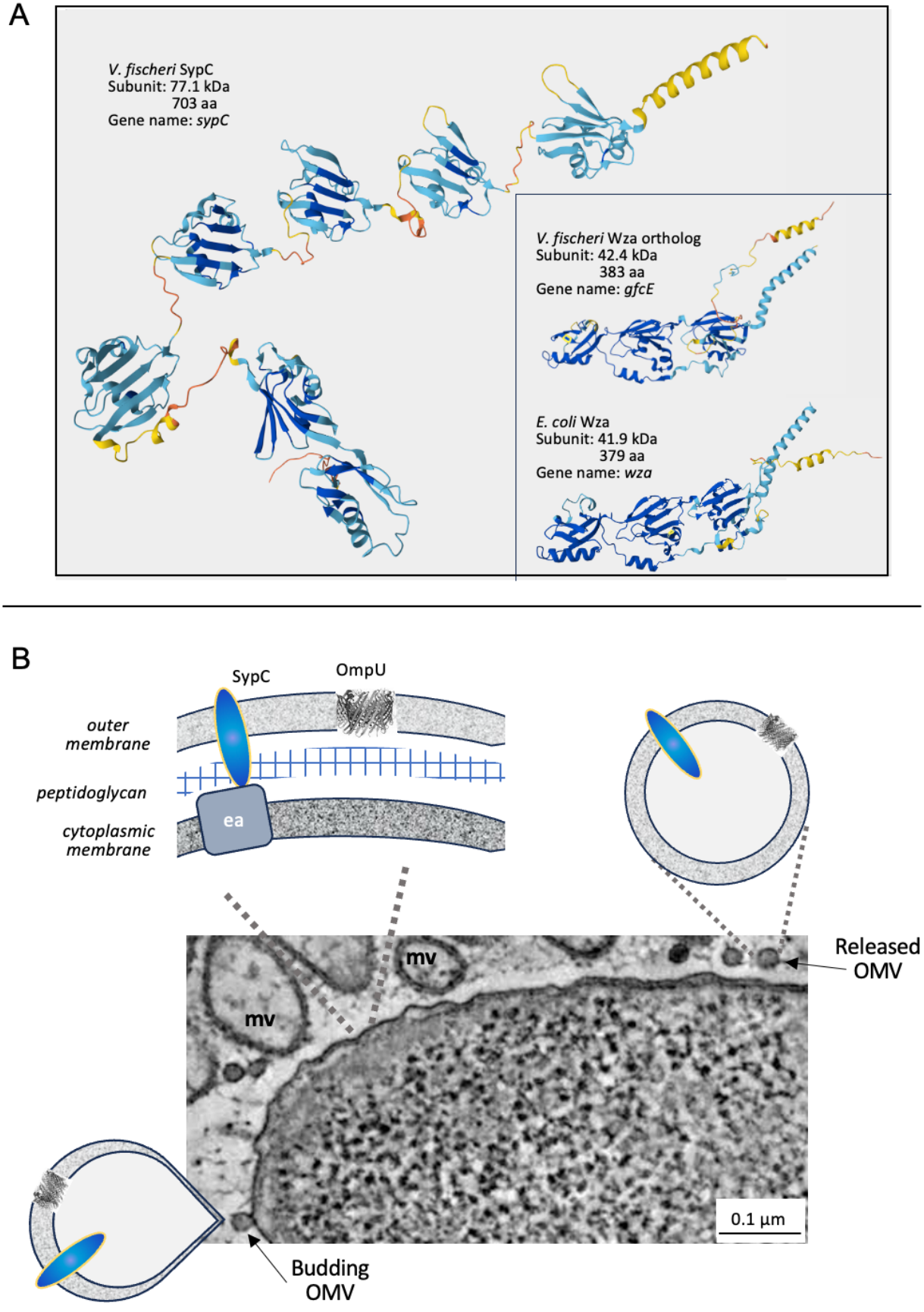
A
V. fischeri SypC
Subunit: 77.1 kDa
703 aa
Gene name: sypC
V. fischeri Wza ortholog
Subunit: 42.4 kDa
383 aa
Gene name: gfcE
E. coli Wza
Subunit: 41.9 kDa
379 aa
Gene name: wza
B
SypC
OmpU
outer membrane
peptidoglycan
cytoplasmic membrane
ea
mv
mv
Released OMV
Budding OMV
0.1 µm

Fig. S1. Characteristics of *V. fischeri* SypC. (*A*) Features of the *V. fischeri S*ypC protein (adapted from UniProt [Universal Protein Resource database]; see Results). SypC-like proteins only occur in closely related *Vibrio* (*Aliivibrio*) spp. *Inset:* Wza, a protein widely occurring in Gram-negative bacteria, is involved in export of exopolysaccharides; *sypC* is likely a paralog of *V. fischeri wza (*aka*, gfcE)*. (*B*) *V. fischeri* OMVs. A transmission electron micrograph of a portion of a *V. fischeri* symbiont surrounded by the microvilli (mv) of the host's crypt epithelial cells. Features the size of OMVs occur associated with (*i.e*., budding) or close to (*i.e*., released) the *V. fischeri* surface. ea, other essential Syp proteins making up the molecular export apparatus for *V. fischeri* Syp exopolysaccharide. OmpU is the major outer membrane porin of *V. fischeri*.

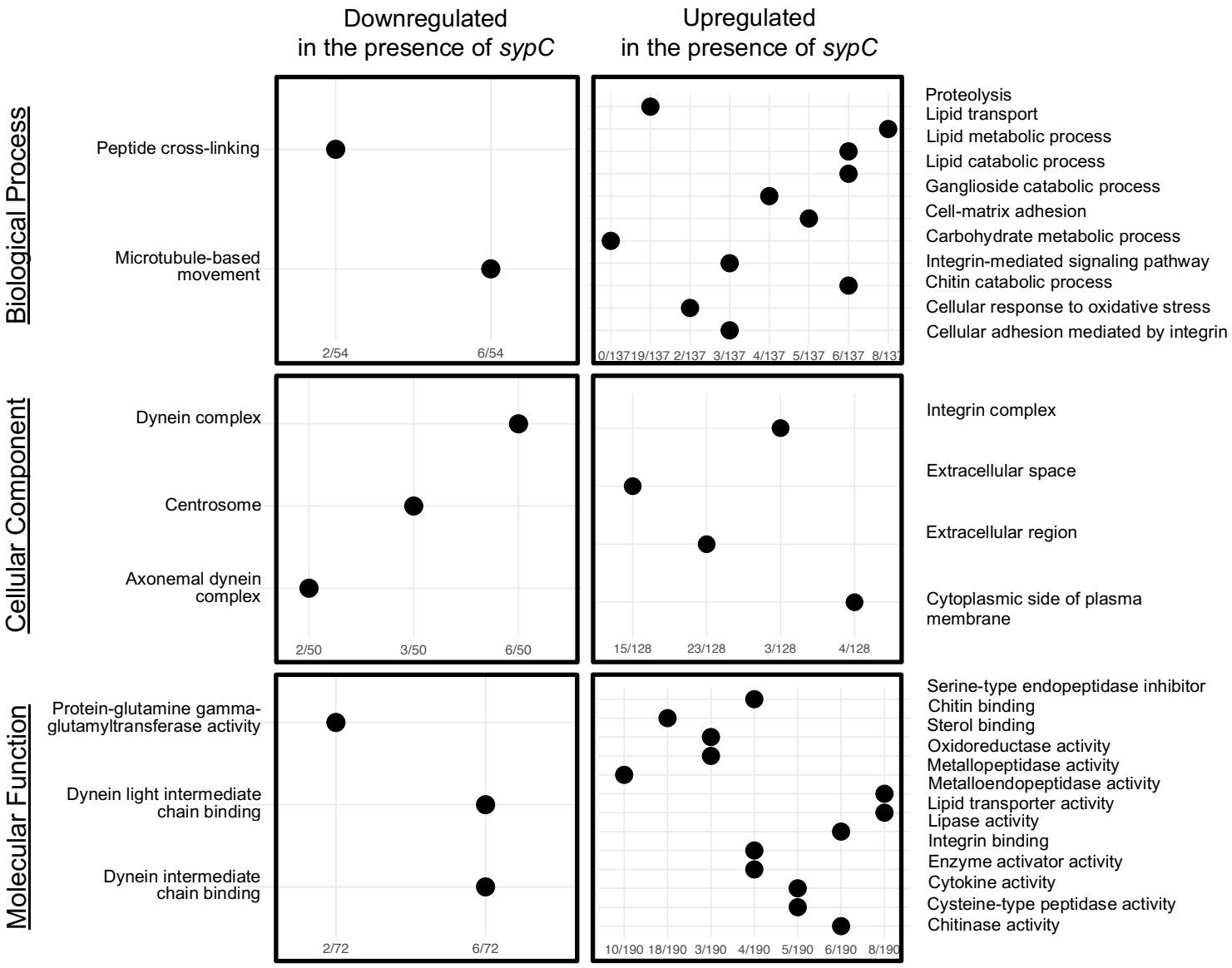

Fig. S2. GO-term enrichment of DEGs. Over-representation analysis (ORA) was performed using Fisher's Exact Test. GO terms shown are significantly enriched among genes that are either downregulated by the presence of the symbiont SypC (Δ*sypC* > WT) or upregulated by SypC (Δ*sypC* < WT). The gene ratio number at the bottom of the data=point columns indicates the proportion of DEGs associated with a given GO term relative to the total number of DEGs tested (*i.e.*, overlapping DEGs / total DEGs in the query set).

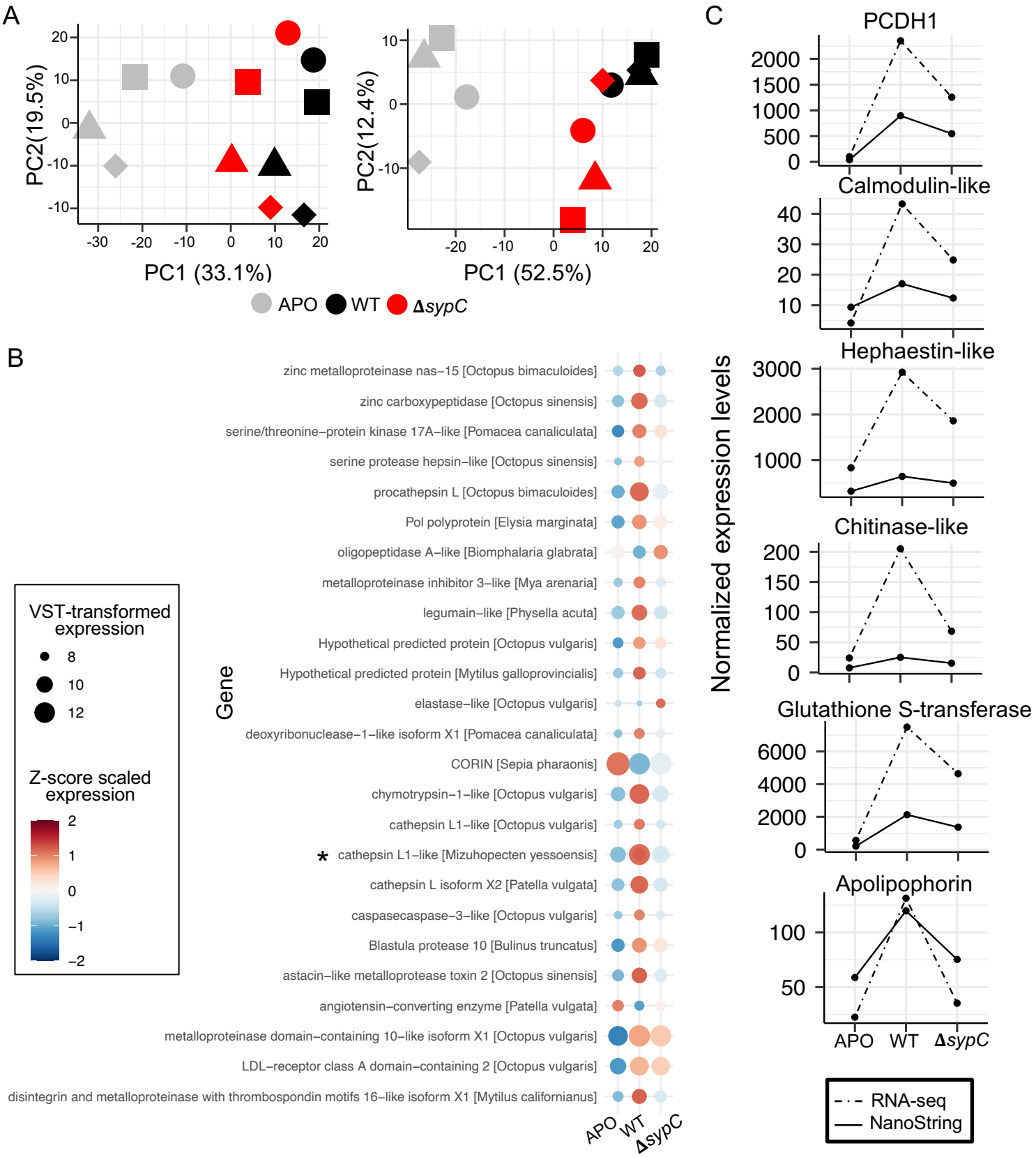
A
PC2(19.5%)
PC1 (33.1%)
PC2(12.4%)
PC1 (52.5%)
APO
WT
ΔsypC
B
Gene
zinc metalloproteinase nas−15 [Octopus bimaculoides]
zinc carboxypeptidase [Octopus sinensis]
serine/threonine−protein kinase 17A−like [Pomacea canaliculata]
serine protease hepsin−like [Octopus sinensis]
procathepsin L [Octopus bimaculoides]
Pol polyprotein [Elysia marginata]
oligopeptidase A−like [Biomphalaria glabrata]
metalloproteinase inhibitor 3−like [Mya arenaria]
legumain−like [Physella acuta]
Hypothetical predicted protein [Octopus vulgaris]
Hypothetical predicted protein [Mytilus galloprovincialis]
elastase−like [Octopus vulgaris]
deoxyribonuclease−1−like isoform X1 [Pomacea canaliculata]
CORIN [Sepia pharaonis]
chymotrypsin−1−like [Octopus vulgaris]
cathepsin L1−like [Octopus vulgaris]
* cathepsin L1−like [Mizuhopecten yessoensis]
cathepsin L isoform X2 [Patella vulgata]
caspasecaspase−3−like [Octopus vulgaris]
Blastula protease 10 [Bulinus truncatus]
astacin−like metalloprotease toxin 2 [Octopus sinensis]
angiotensin−converting enzyme [Patella vulgata]
metalloproteinase domain−containing 10−like isoform X1 [Octopus vulgaris]
LDL−receptor class A domain−containing 2 [Octopus vulgaris]
disintegrin and metalloproteinase with thrombospondin motifs 16−like isoform X1 [Mytilus californianus]
APO
WT
ΔsypC
VST-transformed expression
8
10
12
Z-score scaled expression
2
1
0
−1
−2
C
Normalized expression levels
PCDH1
Calmodulin-like
Hephaestin-like
Chitinase-like
Glutathione S-transferase
Apolipophorin
APO
WT
ΔsypC
RNA-seq
NanoString

Fig. S3. Additional analyses supporting transcriptomic differences. (*A*) PCA plots illustrating the impact of egg clutch (*i.e.*, genetic background) on host-gene expression. *Left*: PCA without clutch modeled as a covariant reveals clustering by genetic background; *right*: PCA with clutch included as a covariant reduces background-driven clustering, supporting the inclusion of clutch in the differential expression model. Four replicates performed, each indicated by a different symbol. (*B*) Differentially expressed genes, most associated with cell death and proteolysis. Asterisk (∗) indicates a cathepsin L gene, whose expression pattern was also examined by NanoString (Fig. 2*D*). (*C*) Comparison of RNA-seq and NanoString expression levels for several additional genes not shown in Fig. 5*D*.

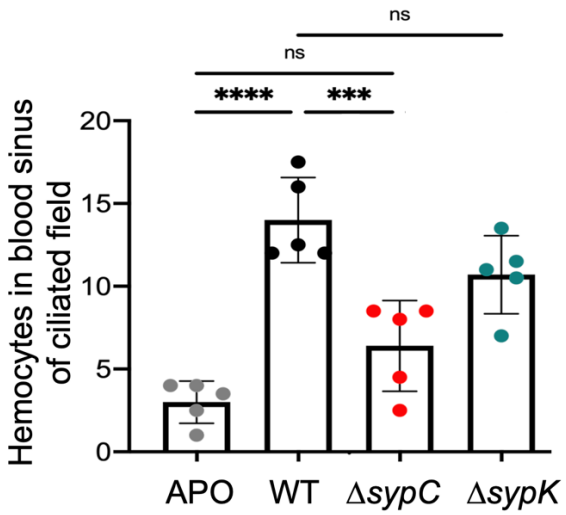

Fig. S4. Normal hemocyte trafficking requires a SypC-specific function other than Syp polysaccharide formation. Quantification of hemocytes in the blood sinus of the anterior appendage at 24 h post-inoculation. Animals were colonized with the WT, Δ*sypC* or Δ*sypK* strain; n=5 per condition. The experiment was repeated 3 times with the same results.

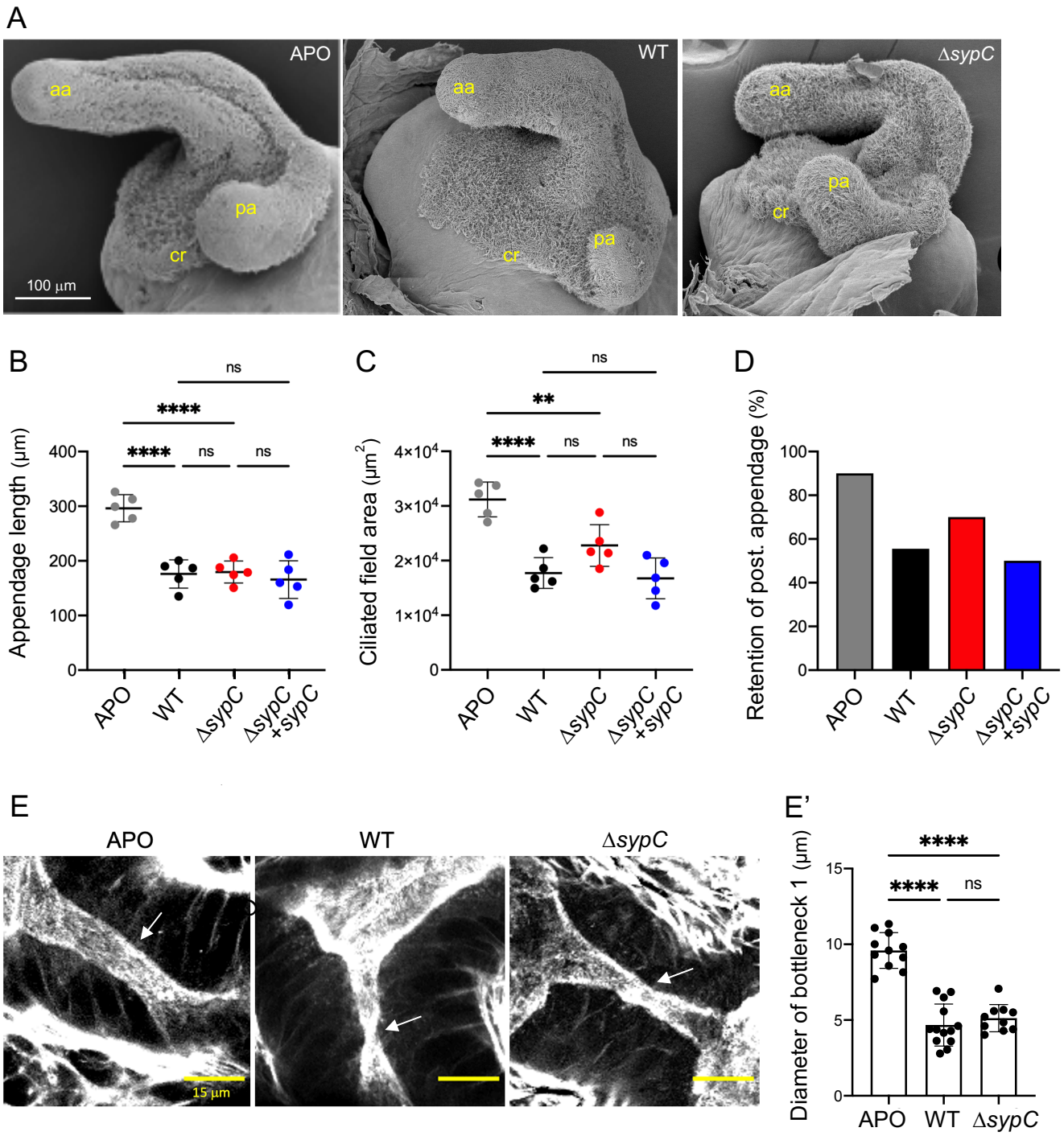

234

235 **Fig. S5.** Patterns of morphogenesis. (*A*) SEM images of the ciliated fields of the light organ at 24
236 hpi, showing the loss of the ciliated ridge (cr) in the wild-type (WT) colonized animal, but its
237 retention in both the aposymbiotic (APO) and Δ*sypC*-colonized animals; aa, anterior appendage;
238 pa, posterior appendage. Measurements of anterior appendage length (*B*) and epithelial-field area

(*C*) at 72 hpi are not significantly different between any of the colonized animal (WT, Δ*sypC,* or the Δ*sypC* +*sypC* complemented strain). Results are the mean ± 1 SD. Comparisons between multiple groups were analyzed using one-way ANOVA with Tukey test. ns: not significant, $P > 0.05$; **$P \leq 0.01$; ****$P \leq 0.0001$. (*D*) Percentage of animals retaining a posterior appendage 72 hpi; n=5 per condition. (*E*) Confocal images of the bottleneck leading into crypt 1 (white arrows) in the migration path between the antechamber and the crypt (see Fig. 1*A'*); the bottleneck constricts to a similar extent in response to colonization by either the WT or Δ*sypC* strain. (*E'*) Quantification of bottleneck diameter at 24 hpi. Each data point represents a biological replicate. Results are the mean ± 1 SD. Comparisons between multiple groups were analyzed using one-way ANOVA with Tukey test. ns: not significant, $P > 0.05$; ****$P \leq 0.0001$.

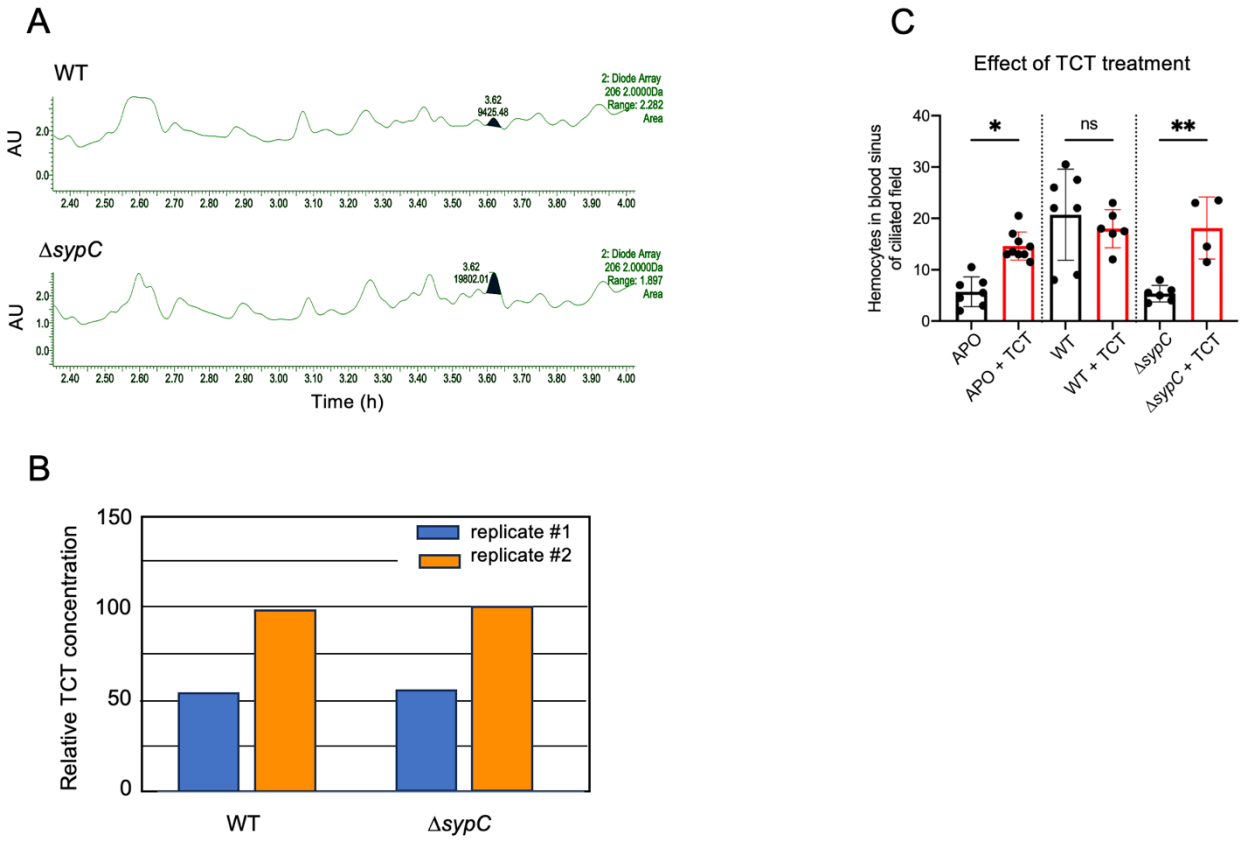

Fig. S6. Effect of a *sypC* deletion on the release of, and host response to, peptidoglycan monomer (TCT). (*A*) Example of HPLC chromatograms comparing the level of TCT released in culture by WT and Δ*sypC V. fischeri* cells. Blackened sections indicate TCT peak areas. AU = relative absorbance units. (*B*) Normalized quantification of TCT exported by cultures of WT or Δ*sypC* in two replicate experiments. (*C*) Quantification of hemocyte number in the blood sinus of the anterior appendage at 24 hpi. Animals were either uncolonized, or colonized with either the WT parent or Δ*sypC* strain, with or without the addition of 1 mM TCT to the surrounding seawater. Each data point represents a biological replicate. Results are the mean ± 1 SD. Comparisons between multiple groups were analyzed using one-way ANOVA with Tukey test. ns: not significant, $P > 0.05$; *$P \leq 0.05$; **$P \leq 0.01$.

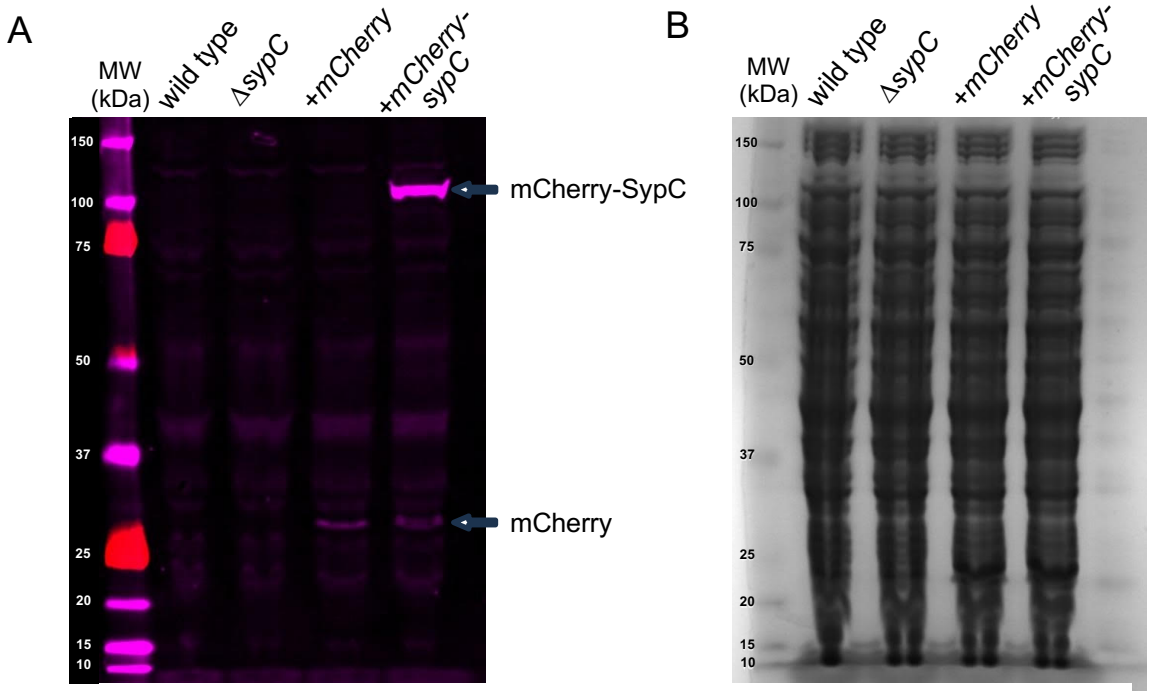
A
MW (kDa)
wild type
ΔsypC
+mCherry
+mCherry-sypC
150
100
75
50
37
25
20
15
10
mCherry-SypC
mCherry
B
MW (kDa)
wild type
ΔsypC
+mCherry
+mCherry-sypC
150
100
75
50
37
25
20
15
10

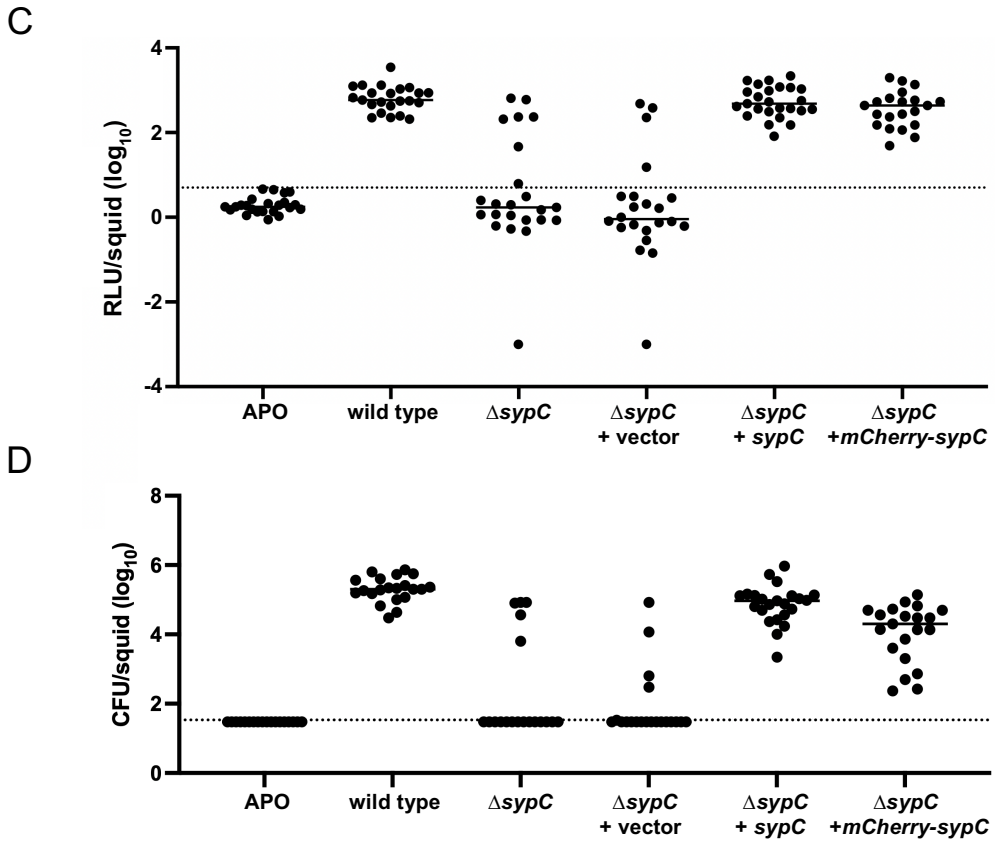
C
RLU/squid (log10)
4
2
0
-2
-4
APO
wild type
ΔsypC
ΔsypC + vector
ΔsypC + sypC
ΔsypC +mCherry-sypC
D
CFU/squid (log10)
8
6
4
2
0
APO
wild type
ΔsypC
ΔsypC + vector
ΔsypC + sypC
ΔsypC +mCherry-sypC

Fig. S7. Detection of the mCherry-SypC fusion protein. (*A*) A fluorescent antibody made to the mCherry protein identified a strongly expressed protein corresponding to the molecular weight of a mCherry-SypC fusion protein. Less strongly expressed was the mCherry protein itself, when encoded on a plasmid used to fluorescently label *V. fischeri* cells. (*B*) Extracts of wild-type or Δ*sypC* strains of *V. fischeri*, as well as strains carrying an mCherry-expressing plasmid or the fusion-protein expressing plasmid, were separated on an SDS-PAGE gel and probed by western blot with the mCherry antibody (*A*). Arrows indicate the expected molecular weights of the fusion protein and the mCherry protein itself. (*C* and *D*) The ability of the *mCherry-sypC* construct to complement a Δ*sypC* mutation in symbiosis. Juvenile squid were either uncolonized (APO) or colonized by wild type *V. fischeri* or one of 4 mutant derivatives. Colonization was a 3-h exposure to 2000-5000 CFU/ml for all conditions except Δ*sypC*, which was an inoculum of 10,000 CFU/ml for 24 h. Phenotypes were scored at 24 h. Colonization success was determined by either (*C*) bioluminescence (relative light units, RLU), or (*D*) CFU per squid. Carriage of an *mCherry-sypC* construct complemented the symbiosis-defective Δ*sypC* mutant essentially as well as a wild-type copy of *sypC*. The dotted lines indicate the limits of detection of each measurement.

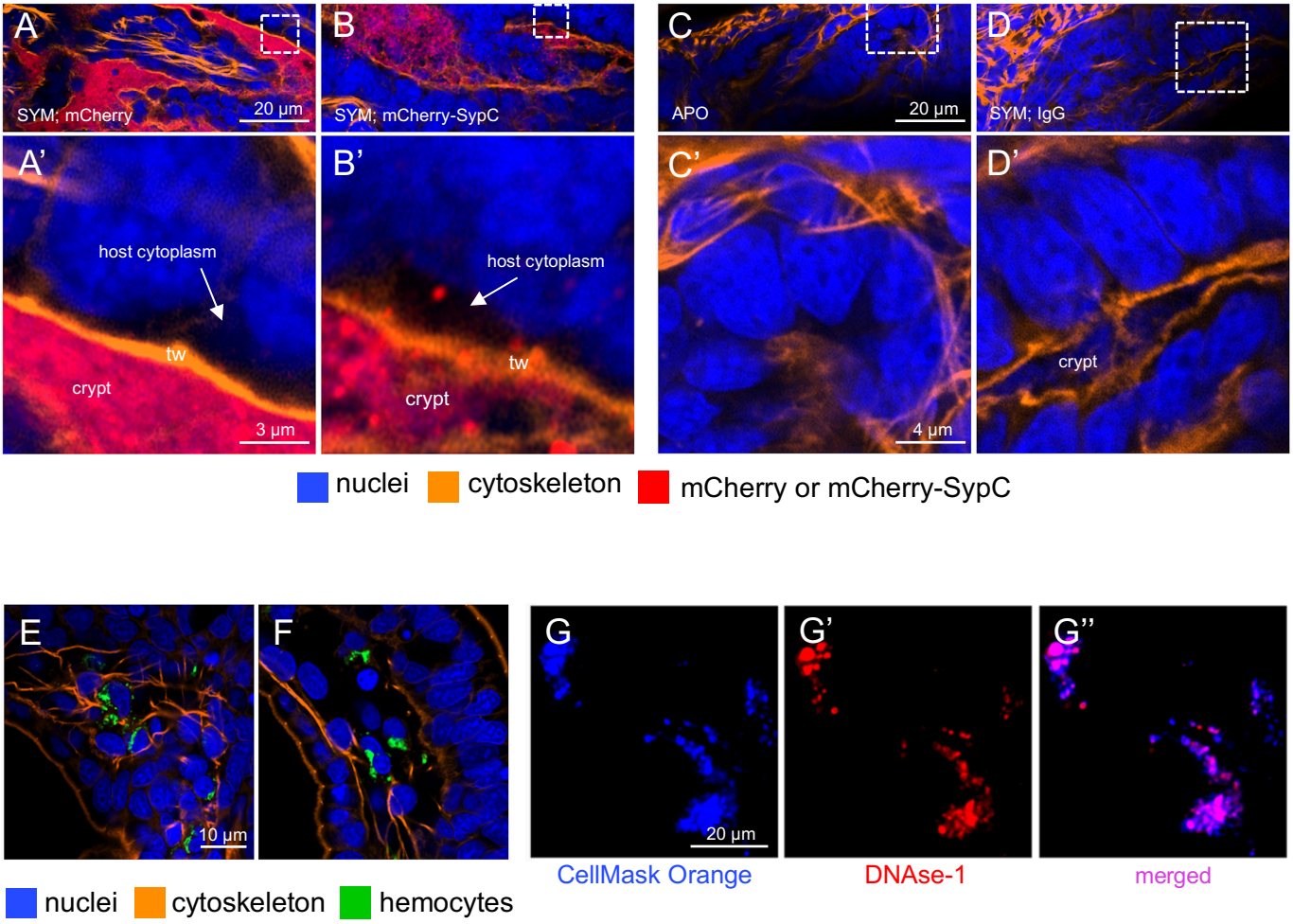

279

280 **Fig. S8.** mCherry-SypC localization. Control images labelled with mCherry antibody supporting
281 the conclusions drawn from Fig. 4. (*A*) Constitutively expressed mCherry protein is confined
282 within the epithelium-lined crypts of a *V. fischeri*-colonized (SYM) host. (*A'*) Enlargement of
283 area in white dashed box. As expected, the bacterium's cytoplasmic mCherry protein remains
284 confined within the symbiont cells and does not appear in the epithelial cell cytoplasm. In
285 contrast, labeling of the mCherry-SypC fusion protein can be seen not only within the symbionts
286 in the crypts (*B*), but also as focused loci located within the host-cell cytoplasm (*B'*). No sign of
287 labeling is seen in either aposymbiotic (APO) tissues treated with fluorescent mCherry antibody
288 (*C*), or in symbiotic tissues treated with control IgG (*D*). Enlargements of areas within the white
289 dashed boxes are below the parent image. Close-up of the blood sinus region of the ciliated
290 anterior appendages of SYM animals (Fig. 1*A'*) treated with either fluorescent mCherry antibody

(*E*) or control IgG (*F*). All tissues were imaged at 22 hpi. nuclei, DAPI (blue); cytoskeleton, rhodamine phalloidin (orange); hemocytes, DNAse-1 (green); antibody to mCherry (red) identifies either the free protein, or the SypC fusion protein; tw, terminal web of the actin cytoskeleton at the outer edge of the host epithelial cells. Colocalization of cell membranes (CellMask Orange; blue) and hemocytes (DNAse-1; red) in the blood sinus (*G-G''*).

Table S1. Strains, plasmids and primers

BACTERIAL STRAINS

Common name	Species/strain	Chromosomal fe	Plasmid	Selection	Description	Reference
ES114	*V. fischeri* ES114	wild type			wild-type squid symbiont	Boettcher & Ruby 1990
ES114mCherry-*sypC*	*V. fischeri* ES114	wild type	pCMC24	Cm 2.5	pCMC24 (*mCherry-sypC* fusion)	this work
ES114 mCherry	*V. fischeri* ES114	wild type	pCMC35	Cm 2.5	pCMC35 (*mCherry*-expressing control for *mCherry* fusions)	this work
ES114 mCherry-*ompU*	*V. fischeri* ES114	wild type	pCMC37	Cm 2.5	pCMC37 (signal peptide-*mCherry-ompU* into ES114	this work
Δ*sypC*	*V. fischeri* ES114	Δ*sypC*			*sypC* mutant	Shibata *et al*. 2012
Δ*sypC* complemented	*V. fischeri* ES114	Δ*sypC*	pSS25	Cm 2.5	*sypC* mutant with native *sypC* complement	Shibata *et al*. 2012
Δ*sypC* vector control	*V. fischeri* ES114	Δ*sypC*	pVSV105	Cm 2.5	*sypC* mutant carrying plasmid vector	this work
Δ*sypC* mCherry-*sypC*	*V. fischeri* ES114	Δ*sypC*	pCMC24	Cm 2.5	*sypC* mutant carrying *mCherry-sypC*	this work
Δ*sypC* mCherry	*V. fischeri* ES114	Δ*sypC*	pCMC35	Cm 2.5	*sypC* mutant carrying *mCherry* label	this work
Δ*ompU* mCherry-*ompU*	*V. fischeri* ES114	Δ*ompU*	pCMC37	Cm 2.5	*ompU* mutant carrying signal peptide-*mCherry-ompU*	this work
DH5α λpir	*E. coli* DH5α λpir	*uidA*::pir+			*E. coli* conjugation strain	Dunn *et al.* 2006
MFDpir	*E. coli* MFDpir	Δ*dapA*::(erm-pir)			DAP deficient *E. coli* for biparental conjugation	Ferrieres *et al*. 2010

PLASMIDS

Name	Selection	Description	Reference
pCMC24	Cm 2.5	pCMC7 with internal ATG deleted in the *mCherry-sypC* fusion	this work
pCMC35	Cm 2.5	pCMC7 with excised *sypC* from *mCherry-sypC* fusion	this work
pCMC37	Cm 2.5	pVSV105 vector with fused signal peptide-*mCherry-ompU*	this work
pSS25	Cm 2.5	native *sypC* complementation plasmid	Shibata et al. 2012
pVSV105	Cm 2.5	*V. fischeri* complementation vector	Dunn *et al*. 2006

PRIMERS

Oligonucleotide ID	Sequence 5' to 3'	Description	Reference
40S-qF3	AAGGCTTTGTCCACCTTCCT	Reference gene S19 ribosomal protein amplification	Moriano- Gutierrez *et al*., 2019
40S-qR3	TAAATGCTCCAACACCAGCA	Reference gene S19 ribosomal protein amplification	Moriano- Gutierrez *et al.*, 2019
C8-qF2	ACGCTCAAAAGGCAGTGG	Target gene C8 subunit of proteasome amplification	this work
C8-qR2	GCCGAACCTATATGCGTATC	Target gene C8 subunit of proteasome amplification	this work

Table S2. Imagining characteristics

Figure	Instrument, upright/inverted	Location	Objective	Detector type	Dyes, Excitation/Emission, laser used
3A	Zeiss LSM 710 upright	Kewalo Marine Laboratory	40x/1.2 water	GaAs-PMT	Acridine orange (502/525 nm), WGA (633 nm)
3B	Zeiss LSM 710 upright	Kewalo Marine Laboratory	40x/1.2 water	GaAs-PMT	DNAse-1 (AF488, 490/525 nm), Rhodamine phalloidin (540/565 nm), TO-PRO-3 (642/661 nm)
4A	Zeiss LSM 900 upright	Caltech, Pasadena, CA	Plan-Apochromatic 63x/1.40 Oil DIC M27	GaAsP-Pmt	GAR-AF647 (650/671 nm), CellMask Orange Plasma Membrane (554/567 nm), DAPI (350/470 nm)
4B (A processed)	Zeiss LSM 900 upright	Caltech, Pasadena, CA	Plan-Apochromatic 63x/1.40 Oil DIC M27	GaAsP-Pmt	GAR-AF647 (650/671 nm), CellMask Orange Plasma Membrane (554/567 nm), DAPI (350/470 nm)
4C (A processed)	Zeiss LSM 900 upright	Caltech, Pasadena, CA	Plan-Apochromatic 63x/1.40 Oil DIC M27	GaAsP-Pmt	GAR-AF647 (650/671 nm), CellMask Orange Plasma Membrane (554/567 nm), DAPI (350/470 nm)
4D	Zeiss LSM 900 upright	Caltech, Pasadena, CA	Plan-Apochromatic 20x/0.8 Air M27	GaAsP-Pmt	GAR-AF647 (650/671 nm), CellMask Orange Plasma Membrane (554/567 nm), DAPI (350/470 nm)
4E-E"	Zeiss LSM 900 upright	Caltech, Pasadena, CA	Plan-Apochromatic 63x/1.40 Oil DIC M27	GaAsP-Pmt	GAR-AF647 (650/671 nm), CellMask Orange Plasma Membrane (554/567 nm), DAPI (350/470 nm)
4F	Zeiss LSM 900 upright	Caltech, Pasadena, CA	Plan-Apochromatic 20x/0.8 Air M27	GaAsP-Pmt	GAR-AF647 (650/671 nm), CellMask Orange Plasma Membrane (554/567 nm), DAPI (350/470 nm)
4G-G"	Zeiss LSM 900 upright	Caltech, Pasadena, CA	Plan-Apochromatic 63x/1.40 Oil DIC M27	GaAsP-Pmt	GAR-AF647 (650/671 nm), CellMask Orange Plasma Membrane (554/567 nm), DAPI (350/470 nm)
5A	Zeiss LSM 900 upright	Caltech, Pasadena, CA	Plan-Apochromatic 40x/1.30 Oil DIC (UV) VIS-IR M27	GaAsP-Pmt	GAR-AF647 (650/671 nm),Rhodamine phalloidin (540/565 nm), DNAse-1 (AF488, 490/525 nm), DAPI (350/470 nm)
5A	Zeiss LSM 900 upright	Caltech, Pasadena, CA	Plan-Apochromatic 40x/1.30 Oil DIC (UV) VIS-IR M27	GaAsP-Pmt	GAR-AF647 (650/671 nm),Rhodamine phalloidin (540/565 nm), DNAse-1 (AF488, 490/525 nm), DAPI (350/470 nm)
5A	Zeiss LSM 900 upright	Caltech, Pasadena, CA	Plan-Apochromatic 40x/1.30 Oil DIC (UV) VIS-IR M27	GaAsP-Pmt	GAR-AF647 (650/671 nm),Rhodamine phalloidin (540/565 nm), DNAse-1 (AF488, 490/525 nm), DAPI (350/470 nm)
5A	Zeiss LSM 900 upright	Caltech, Pasadena, CA	Plan-Apochromatic 40x/1.30 Oil DIC (UV) VIS-IR M27	GaAsP-Pmt	GAR-AF647 (650/671 nm),Rhodamine phalloidin (540/565 nm), DNAse-1 (AF488, 490/525 nm), DAPI (350/470 nm)
5A	Zeiss LSM 900 upright	Caltech, Pasadena, CA	Plan-Apochromatic 40x/1.30 Oil DIC (UV) VIS-IR M27	GaAsP-Pmt	GAR-AF647 (650/671 nm),Rhodamine phalloidin (540/565 nm), DNAse-1 (AF488, 490/525 nm), DAPI (350/470 nm)
S6A	Hitachi S-4800	University of Hawaii-Manoa	400x	none	none
S6E	Zeiss LSM 710 upright	Kewalo Marine Laboratory	40x/1.2 water	GaAs-PMT	DNAse-1 (AF488, 490/525 nm), Rhodamine phalloidin (540/565 nm), TO-PRO-3 (642/661 nm)
S9A-A'	Zeiss LSM 900 upright	Caltech, Pasadena, CA	Plan-Apochromatic 40x/1.30 Oil DIC (UV) VIS-IR M27	GaAsP-Pmt	GAR-AF647 (650/671 nm),Rhodamine phalloidin (540/565 nm), DAPI (350/470 nm)
S9A-A'	Zeiss LSM 900 upright	Caltech, Pasadena, CA	Plan-Apochromatic 40x/1.30 Oil DIC (UV) VIS-IR M27	GaAsP-Pmt	GAR-AF647 (650/671 nm),Rhodamine phalloidin (540/565 nm), DAPI (350/470 nm)
S9A-A'	Zeiss LSM 900 upright	Caltech, Pasadena, CA	Plan-Apochromatic 40x/1.30 Oil DIC (UV) VIS-IR M27	GaAsP-Pmt	GAR-AF647 (650/671 nm),Rhodamine phalloidin (540/565 nm), DAPI (350/470 nm)
S9A-A'	Zeiss LSM 900 upright	Caltech, Pasadena, CA	Plan-Apochromatic 40x/1.30 Oil DIC (UV) VIS-IR M27	GaAsP-Pmt	GAR-AF647 (650/671 nm),Rhodamine phalloidin (540/565 nm), DAPI (350/470 nm)
S9A-A'	Zeiss LSM 900 upright	Caltech, Pasadena, CA	Plan-Apochromatic 40x/1.30 Oil DIC (UV) VIS-IR M27	GaAsP-Pmt	GAR-AF647 (650/671 nm),Rhodamine phalloidin (540/565 nm), DNAse-1 (AF488, 490/525 nm), DAPI (350/470 nm)
S9A-A'	Zeiss LSM 900 upright	Caltech, Pasadena, CA	Plan-Apochromatic 40x/1.30 Oil DIC (UV) VIS-IR M27	GaAsP-Pmt	GAR-AF647 (650/671 nm),Rhodamine phalloidin (540/565 nm), DNAse-1 (AF488, 490/525 nm), DAPI (350/470 nm)
S9A-A'	Zeiss LSM 900 upright	Caltech, Pasadena, CA	Plan-Apochromatic 40x/1.30 Oil DIC (UV) VIS-IR M27	GaAsP-Pmt	DNAse-1 (AF488, 490/525 nm), CellMask Orange Plasma Membrane (554/567 nm), DAPI (350/470 nm)

Table S2. Imagining characteristics (page 2)

Figure	Track: laser wavelength, gain, detection wavelength	Averaging, bit depth	Snap or Z-stack
3A		4, 16	Z-stack
3B	Track 1: (AF647) 640 nm, 1.2%, 591V, 645-700, Track 2: (Rhodamine) 561 nm, 0.04%, 500V, 410-647, Track 3: (FITC) 488 nm, 0.10%, 500V, 410-546, Track 4: (DAPI) 405 nm, 0.1%, 500V, 400-490	4, 16	Z-stack
4A	Track 1: (AF647) 640 nm, 0.2%, 591V, 645-700, Track 2: (CMO) 561 nm, 0.5%, 500V, 410-647, Track 3: (DAPI) 405 nm, 0.3%, 500V, 400-490	4, 16	Z-stack, 0.5um steps
4B (A processed)	Track 1: (AF647) 640 nm, 0.2%, 591V, 645-700, Track 2: (CMO) 561 nm, 0.5%, 500V, 410-647, Track 3: (DAPI) 405 nm, 0.3%, 500V, 400-490	4, 16	Z-stack, 0.5um steps
4C (A processed)	Track 1: (AF647) 640 nm, 0.2%, 591V, 645-700, Track 2: (CMO) 561 nm, 0.5%, 500V, 410-647, Track 3: (DAPI) 405 nm, 0.3%, 500V, 400-490	4, 16	Z-stack, 0.5um steps
4D	Track 1: (AF647) 640 nm, 0.2%, 591V, 645-700, Track 2: (CMO) 561 nm, 0.5%, 500V, 410-647, Track 3: (DAPI) 405 nm, 0.3%, 500V, 400-490	4, 16	Z-stack, 0.5um steps
4E-E"	Track 1: (AF647) 640 nm, 0.2%, 591V, 645-700, Track 2: (CMO) 561 nm, 0.5%, 500V, 410-647, Track 3: (DAPI) 405 nm, 0.3%, 500V, 400-490	4, 16	Z-stack, 0.5um steps
4F	Track 1: (AF647) 640 nm, 0.2%, 591V, 645-700, Track 2: (CMO) 561 nm, 0.5%, 500V, 410-647, Track 3: (DAPI) 405 nm, 0.3%, 500V, 400-490	4, 16	Z-stack, 0.5um steps
4G-G"	Track 1: (AF647) 640 nm, 0.2%, 591V, 645-700, Track 2: (CMO) 561 nm, 0.5%, 500V, 410-647, Track 3: (DAPI) 405 nm, 0.3%, 500V, 400-490	4, 16	Z-stack, 0.5um steps
5A	Track 1: (AF647) 640 nm, 0.2%, 591V, 645-700, Track 2: (Rhodamine) 561 nm, 0.03%, 500V, 410-617, Track 3: (FITC) 488 nm, 0.10%, 500V, 410-546, Track 4: (DAPI) 405 nm, 0.2%, 500V, 400-490	4, 16	Z-stack, 0.5um steps
5A	Track 1: (AF647) 640 nm, 0.2%, 591V, 645-700, Track 2: (Rhodamine) 561 nm, 0.03%, 500V, 410-617, Track 3: (FITC) 488 nm, 0.10%, 500V, 410-546, Track 4: (DAPI) 405 nm, 0.2%, 500V, 400-490	4, 16	Z-stack, 0.5um steps
5A	Track 1: (AF647) 640 nm, 0.2%, 591V, 645-700, Track 2: (Rhodamine) 561 nm, 0.03%, 500V, 410-617, Track 3: (FITC) 488 nm, 0.10%, 500V, 410-546, Track 4: (DAPI) 405 nm, 0.2%, 500V, 400-490	4, 16	Z-stack, 0.5um steps
5A	Track 1: (AF647) 640 nm, 0.2%, 591V, 645-700, Track 2: (Rhodamine) 561 nm, 0.03%, 500V, 410-617, Track 3: (FITC) 488 nm, 0.10%, 500V, 410-546, Track 4: (DAPI) 405 nm, 0.2%, 500V, 400-490	4, 16	Z-stack, 0.5um steps
5A	Track 1: (AF647) 640 nm, 0.2%, 591V, 645-700, Track 2: (Rhodamine) 561 nm, 0.03%, 500V, 410-617, Track 3: (FITC) 488 nm, 0.10%, 500V, 410-546, Track 4: (DAPI) 405 nm, 0.2%, 500V, 400-490	4, 16	Z-stack, 0.5um steps
S6A	none	none	Snap
S6E	Track 1: (AF647) 640 nm, 1.2%, 591V, 645-700, Track 2: (Rhodamine) 561 nm, 0.04%, 500V, 410-647, Track 3: (FITC) 488 nm, 0.10%, 500V, 410-546, Track 4: (DAPI) 405 nm, 0.1%, 500V, 400-490	4, 16	Z-stack
S9A-A'	Track 1: (AF647) 640 nm, 1.2%, 591V, 645-700, Track 2: (Rhodamine) 561 nm, 0.04%, 500V, 410-647, Track 3: (FITC) 488 nm, 0.10%, 500V, 410-546, Track 4: (DAPI) 405 nm, 0.1%, 500V, 400-490	4, 16	Snap
S9A-A'	Track 1: (AF647) 640 nm, 0.5%, 591V, 645-700, Track 2: (Rhodamine) 561 nm, 0.03%, 500V, 410-617, Track 3: (FITC) 488 nm, 0.10%, 500V, 410-546, Track 4: (DAPI) 405 nm, 0.2%, 500V, 400-490	4, 16	Z-stack, 0.5um steps
S9A-A'	Track 1: (AF647) 640 nm, 0.2%, 591V, 645-700, Track 2: (Rhodamine) 561 nm, 0.03%, 500V, 410-617, Track 3: (FITC) 488 nm, 0.10%, 500V, 410-546, Track 4: (DAPI) 405 nm, 0.2%, 500V, 400-490	4, 16	Snap
S9A-A'	Track 1: (AF647) 640 nm, 0.2%, 591V, 645-700, Track 2: (Rhodamine) 561 nm, 0.03%, 500V, 410-617, Track 3: (FITC) 488 nm, 0.10%, 500V, 410-546, Track 4: (DAPI) 405 nm, 0.2%, 500V, 400-490	4, 16	Snap
S9A-A'	Track 1: (AF647) 640 nm, 0.2%, 591V, 645-700, Track 2: (Rhodamine) 561 nm, 0.03%, 500V, 410-617, Track 3: (FITC) 488 nm, 0.10%, 500V, 410-546, Track 4: (DAPI) 405 nm, 0.2%, 500V, 400-490	4, 16	Snap
S9A-A'	Track 1: (AF647) 640 nm, 0.2%, 591V, 645-700, Track 2: (Rhodamine) 561 nm, 0.03%, 500V, 410-617, Track 3: (FITC) 488 nm, 0.10%, 500V, 410-546, Track 4: (DAPI) 405 nm, 0.2%, 500V, 400-490	4, 16	Snap
S9A-A'	Track 1: (CMO) 561 nm, 2%, 500V, 535-617, Track 2: (AF488) 488 nm, 0.5%, 500V, 410-546, Track 3: (DAPI) 405 nm, 0.6%, 500V, 400-495	4, 16	Snap

SI References

1. B. D. Bennett, T. Essock-Burns, E. G. Ruby, HbtR, a heterofunctional homolog of the virulence regulator TcpP, facilitates the transition between symbiotic and planktonic lifestyles in *Vibrio fischeri*. *mBio* **11** (2020).
2. J. Graf, P. V. Dunlap, E. G. Ruby, Effect of transposon-induced motility mutations on colonization of the host light organ by *Vibrio fischeri*. *J Bacteriol* **176**, 6986-6991 (1994).
3. K. J. Boettcher, E. G. Ruby, Detection and quantification of *Vibrio fischeri* autoinducer from symbiotic squid light organs. *J Bacteriol* **177**, 1053-1058 (1995).
4. L. Yang *et al.*, Bacterial growth dynamics in a rhythmic symbiosis. *Mol Biol Cell* **35**, ar79 (2024).
5. A. K. Dunn, D. S. Millikan, D. M. Adin, J. L. Bose, E. V. Stabb, New rfp- and pES213-derived tools for analyzing symbiotic *Vibrio fischeri* reveal patterns of infection and *lux* expression *in situ*. *Appl Environ Microbiol* **72**, 802-810 (2006).
6. K. L. Visick, K. M. Hodge-Hanson, A. H. Tischler, A. K. Bennett, V. Mastrodomenico, Tools for rapid genetic engineering of *Vibrio fischeri*. *Appl Environ Microbiol* **84** (2018).
7. L. Ferrieres *et al.*, Silent mischief: bacteriophage Mu insertions contaminate products of *Escherichia coli* random mutagenesis performed using suicidal transposon delivery plasmids mobilized by broad-host-range RP4 conjugative machinery. *J Bacteriol* **192**, 6418-6427 (2010).
8. D. N. Mastronarde, S. R. Held, Automated tilt series alignment and tomographic reconstruction in IMOD. *J Struct Biol* **197**, 102-113 (2017).
9. J. R. Kremer, D. N. Mastronarde, J. R. McIntosh, Computer visualization of three-dimensional image data using IMOD. *J Struct Biol* **116**, 71-76 (1996).
10. D. N. Mastronarde, Correction for non-perpendicularity of beam and tilt axis in tomographic reconstructions with the IMOD package. *J Microsc* **230**, 212-217 (2008).
11. J. B. Lynch *et al.*, Ambient pH alters the protein content of outer membrane vesicles, driving host development in a beneficial symbiosis. *J Bacteriol* **201** (2019).
12. S. Moriano-Gutierrez *et al.*, The noncoding small RNA SsrA is released by *Vibrio fischeri* and modulates critical host responses. *PLoS Biol* **18**, e3000934 (2020).

13. S. Moriano-Gutierrez *et al.*, Critical symbiont signals drive both local and systemic changes in diel and developmental host gene expression. *Proc Natl Acad Sci U S A* **116**, 7990-7999 (2019).
14. K. J. Livak, T. D. Schmittgen, Analysis of relative gene expression data using real-time quantitative PCR and the 2(-delta delta C(T)) method. *Methods* **25**, 402-408 (2001).